Yanbu Journal of Engineering and Science

Volume 23 | Issue 1 Article 2

2026

Direct Current Servo Motor Speed Characterization Using Proportional and Integral Controllers

Adel S. Bahakeem
Electrical Engineering Department, Jubail Industrial College, Jubail Industrial City 31961, Saudi Arabia

Ahmad Jamal
Mechanical Engineering Department, Jubail Industrial College, Jubail Industrial City 31961, Saudi Arabia, jamalah@rcjy.edu.sa

Mir M. M. Morshed
Mechanical Engineering Department, Jubail Industrial College, Jubail Industrial City 31961, Saudi Arabia

Elwaleed A. Khidir
Mechanical Engineering Department, Jubail Industrial College, Jubail Industrial City 31961, Saudi Arabia

Follow this and additional works at: https://yjes.researchcommons.org/yjes

The journal in which this article appears is hosted on Digital Commons, an Elsevier platform.

Recommended Citation

Bahakeem, Adel S.; Jamal, Ahmad; Morshed, Mir M. M.; and Khidir, Elwaleed A. (2026), Direct Current Servo Motor Speed Characterization Using Proportional and Integral Controllers, *Yanbu Journal of Engineering and Science*: Vol. 23: Iss. 1, 26-51.
DOI: https://doi.org/10.53370/1658-5321.1208
Available at: https://yjes.researchcommons.org/yjes/vol23/iss1/2

This Research Article is brought to you for free and open access by Yanbu Journal of Engineering and Science. It has been accepted for inclusion in Yanbu Journal of Engineering and Science by an authorized editor of Yanbu Journal of Engineering and Science.

YANBU JOURNAL OF ENGINEERING AND SCIENCE 2025;23:26–51

Scan the QR to view the full-text article on the journal website

RESEARCH ARTICLE

Direct Current Servo Motor Speed Characterization Using Proportional and Integral Controllers

Adel S. Bahakeem [a], **Ahmad Jamal** [b,*], **Mir M. M. Morshed** [b], **Elwaleed A. Khidir** [b]

[a] Electrical Engineering Department, Jubail Industrial College, Jubail Industrial City 31961, Saudi Arabia
[b] Mechanical Engineering Department, Jubail Industrial College, Jubail Industrial City 31961, Saudi Arabia

ABSTRACT

The present study is focused on investigating the steady-state and transient responses of a DC servo motor controlled by the Proportional and Integral controllers. It is also studied how the P and I controllers affect the stability, error, and damping of the DC motor response. The DC servo motor responses are obtained experimentally using a servo trainer and a PI analog controller, and theoretically using MATLAB Simulink. It is found through the results that the P controller contributes to decreasing the input-output errors of steady-state and transient responses and tends to stabilize the system. It also speeds up the system response. On the other hand, the I controller tends to diminish the error but with sluggish response and affects the system's stability with oscillations. Also, the Simulink results show that the optimized PI controller gains ($K_p = 1.0363$ and $K_i = 1.9438$) significantly reduce the overshoot and settling time. Through the present work, it is desired to obtain a stable response of the DC servo motor to the steady-state and transient input signals. The novelty of the present work is developing a PI controller-based nonlinear model for the DC servo motor speed control and optimizing the PI controller gains for the motor's optimum performance.

Keywords: P controller, I controller, Direct current servo motor, MATLAB simulink, Controller gain optimization

1. Introduction

A DC servo motor is an equipment that is usually required in applications where precise control of speed, direction, and position is required. The speed of the DC servo motor, for instance, becomes very important in applications such as Computer Numerically Controlled (CNC) machines for metal cutting, packaging, material handling, door opening, printing, etc. For such a purpose, a DC servo motor is required to produce the desired speed accurately. In many cases, the speed produced by the DC motor is not the same as the required speed. For this purpose, controllers are used to minimize the difference or error between the actual and desired speeds. Proportional (P), Integral (I), and Derivative (D) controllers, or simply PID controllers, are one of the effective controllers to achieve this. Through these controllers, the output speed of the DC motor is continuously checked against the required speed, and through a feedback system, an error correction algorithm keeps adjusting the power required to obtain the desired speed.

PID controllers are widespread and widely used in industrial systems applications. It is reported that more than ninety-five percent of the controllers used are PID because they work well in many different operating conditions [1]. Despite their simplicity and robustness, many of these controllers are not properly tuned. This makes the topic highly appealing to academic scholars [2]. The majority of these controllers are PI type, as the derivative effect is not used for many applications due to the noise in the control process [3]. Therefore, a PI controller is mostly preferred in many applications instead of a PID. The PI controller is used in applications where the speed of system response and minimum response

Received 29 June 2025; revised 30 September 2025; accepted 15 October 2025.
Available online 30 October 2025

* Corresponding author.
E-mail address: jamalah@rcjy.edu.sa (A. Jamal).

https://doi.org/10.53370/1658-5321.1208
1658-5321/© 2025 The Author(s). Yanbu Journal of Engineering and Science. This is an open access article under the CC BY 4.0 Licence (https://creativecommons.org/licenses/by/4.0/).
Published by Yanbu Industrial College, Saudi Arabia. The journal is hosted on Digital Commons, an Elsevier Platform.

error, i.e., deviation from the desired set value of process variables subjected to any rapid change in the input parameters, is a prime concern. One of the applications is the inlet valve control through the PI controller to supply the desired amount of gas to the burner so that the set temperature of the water can be provided to the process. The PI controller ensures a rapid opening and closing of the inlet valve without much deviation from the required opening of the valve. Similarly, a PI controller is also used in the active control of the twin-accumulator suspension system of an automobile [4]. Another application of the PI controller is the electric propulsion system in model aircraft. The principal components of the system are the battery, Electronic Speed Controller (ESC), Throttle Pulse Width Moderator (PWM), motor, propeller, and PI controller. The desired usage of the battery power is set in the PI controller. While in use, the controller receives the current and voltage usage from the battery and calculates the power drawn from the battery. Based on the error between the power measured and the desired power designated as the set point, the output signal from the controller then adjusts the throttle to bring the battery usage to the desired power level.

Each of the Proportional (P), Integral (I), and Derivative (D) controllers has specific advantages and disadvantages. P controller is usually used in first-order systems/processes with sole energy storage to stabilize the unstable process. It decreases steady-state error, improves system stability, which is associated to a bounded controlled output of a closed-loop system that eventually converges to a constant desired setpoint value in response to a disturbance or any change in the setpoint value, enhances speed of response, and reduces rise time. Some of its disadvantages include long settling time, inability to eliminate steady-state error, an increase in maximum overshoot of the system response, and suitability to first-order systems only. I controller has a major advantage of eliminating the steady-state error or offset between the set point and the system output. On the other hand, the I controller reduces the speed of system response, affects the system stability, and has a poor transient response that results in oscillations. In contrast to the I controller, the D controller improves the transient response of the system, and decreases the settling time and oscillations. D controller, however, is never used alone because it directly amplifies the process high frequency noise. It never reduces the steady-state error and causes the system response time to increase. Using a combination of these controllers, the combined advantages of individual controllers can be utilized. For instance, a PI controller has the advantage of eliminating steady-state error without affecting the stability of the system and reducing rise time, resulting in faster response of the system. However, the disadvantages of PI controllers can be a narrower range of stability, high initial overshoot, controller gain sensitivity, and lethargic response to abrupt perturbations. A commonly used control system containing all P, I, and D controllers has the advantages of quicker response time due to reduced time constant, zero offset or error, and improved stability of the system. The downside of the PID system is that it is the most expensive as compared to the individual control systems, can be unstable if not tuned properly, susceptible to noise magnification, may sustain oscillations around the desired output, and repeated tuning may reduce its life span.

The utilization of a PID controller to achieve speed and direction control of different types of motors has been studied extensively in the past. Sinthipsomboon et al. [5] proposed a fuzzy and hybrid fuzzy self-tuning PID controller for the speed control of a servo-controlled hydraulic motor, also called Servo Electro Hydraulic System (SEHS), and tested it experimentally. They utilized the controller in two parts; a fuzzy controller was used in case of the system output substantially far from the set output value, and a fuzzy self-tuning PID in case of the output close to the set value. Their hybrid controller showed superior performance compared to the hybrid fuzzy and PID controller. Similar results were obtained by Lan [6], who also proved through experiments on SEHS that fuzzy and hybrid fuzzy self-tuning PID controller has superior performance over the hybrid fuzzy and PID controller. Korayem et al. [7] proposed a theoretical model that used PID controllers and the Pulse Width Modulation (PWM) method to concurrently regulate the speed and torque of the motors of a cable-suspended robot. The feedback capability of the PID controller was utilized to control the voltage for the speed and current for the torque of the motor. The feed-forward term of the model was used to improve the response of the motors. They established the adequacy of the proposed model with the help of experiments. Another class of PID controller, a simplified Fractional Order Proportional Integral Derivative (FOPID) controller, was proposed by Zheng et al. [8]. On the basis of their previous work [9], they improved the FOPID controller by developing a nonlinear correlation between the integral and derivative gains K_i and K_d, respectively, with a variable coefficient. With the proposed estimation model, they found that the optimal FOPID controller parameters could be found analytically. They applied their proposed model to the Permanent Magnet Synchronous Motor (PMSM) and found that the motor

using the proposed model obtained better step response performance. In the same year, Ekinci et al. [10] optimized the FOPID controller parameters to regulate the speed of a DC motor using a novel metaheuristic approach, i.e., the Opposition-Based (OBL) hybrid Manta Ray Foraging Optimization (MRFO) with Simulated Annealing (SA) algorithm. They also validated their proposed optimization algorithm with the experimental results and compared it with other advanced algorithms, and found that their proposed algorithm outperformed the others in terms of the performance parameters such as steady-state error, rise time, settling time, and maximum overshoot.

Ali et al. [11] implemented the Field Programmable Gate Array (FPGA) module of LabVIEW to design a digital system to regulate the speed of a DC motor. The digital system included a circuit to extract the set point value and process variable, a PID controller, and a PWM signal generator. They implemented their digital LabVIEW system on a physical system, namely, Spartan-3E FPGA Xilinx. A very interesting comparative analysis between the conventional Integer Order (IO) and Fractional Order (FO)-based PID controller to control the speed of a chopper-fed DC motor was conducted by Rajasekhar et al. [12]. A new opposition-based Artificial Bee Colony (ABC) algorithm for the PID parameters optimization was used for both types of controllers. It was found that FOPID outperformed the conventional IOPID. Dawood et al. [13] used a traditional PID controller to control the speed of a three-phase four-pole multi-PMSM by means of a mathematical model. A master/slave approach was used for the motor speed control. Simulations of the model were done in a MATLAB Simulink environment. They found that their control method could control the multi-PMSM effectively. Similarly, various optimization algorithms were tested by the researchers to adjust the PID controller parameters for effective speed regulation of different types of motors [14–20]. More recently, Liu and Bai [21] proposed a PID controller based Back-Propagation neural network model to regulate the speed of an asynchronous AC motor. Through the model, they could find the K_p, K_i, and K_d nonlinear coupling law and improve PID controller performance. Another related work proposed an Adaptive Fuzzy-Neural Fast Terminal Synergetic Controller (AFN-FTSC) to monitor the load voltage coupled to a buck DC/DC converter [22].

To enhance the speed regulation of the DC servo motor, Swami and Gaur [23] utilized an Improved self-tuning fuzzy (ISTF) PID controller in which fuzzy logic was utilized to adjust the PID controller gains. The main aim of the research, in general, is to tune the controller parameter gains for a better dynamic and steady-state response of the motor under varying load conditions [24–26]. Kumar and Mittal [27] recently used a PID controller and the parameter tuning algorithms such as GA and ZN to efficiently regulate the speed of a DC servo motor under controlled perturbations. They found that GA better controls the frequency response of the motor as compared to ZN.

There are substantial studies in which the PI controller was employed to regulate the speed of different types of motors. It is a matter of how efficiently the controller enhances the performance of the motor. One of these studies is by Polsena et al. [28] who implemented the PSO algorithm and a one-dimensional Kalman filter for obtaining the optimized PI controller parameters. These parameters were fed into the physical motor system and compared with the simulated results. Kociszewski [29], on the other hand, implemented the analogue PI controller in the re-programmable microcontroller from the PSoC1 family to control the DC motor speed acting as a mobile robot drive. Another work by Yustin et al. [30] implemented a cascade PI controller in series connection in a DC motor and tuned its controller gains with the help of PSO and GA algorithms. Later, they compared the simulation results with those of the experiments and found the agreement satisfactory. Sundareswaran and Vasu [31] tuned the PI controller gain parameters with the help of GA and simulated the motor speed response against an input signal using these tuned parameters. The results validated the optimization model. Many researchers focused their attention on finding the most suitable tuning method that gave the optimized PI controller gain parameters for the speed control of DC motors [32–41]. Recent studies by Mansor et al. [42] and Samat et al. [43] suggested a self-tuning Fuzzy Logic Control (FLC) and PSO technique to obtain the optimized PI controller gains for effective speed control of a DC motor, respectively. They found in their perspectives that both techniques produced improved system response in terms of faster rise time, lesser speed error, and enhanced dynamic response. The ever-growing use of Artificial Intelligence (AI) /machine learning can be seen in the PI controller design. For instance, two recent studies by Tufenkci et al. [44] and Sanjines et al. [45] demonstrated Reinforcement Learning (RL) based PI controller design for the speed control of DC motors. Both of them made use of Neural Network (NN) to train the actor-critic agent in a MATLAB Simulink environment and focused on obtaining a rapid DC motor response by using the Twin Delay Deep Deterministic (TD3) policy gradient method within the NN. In the former work, the results were compared with those of other conventional methods such as GA and FOPI. In the latter work, the results were compared with those of

classical control techniques using the MATLAB Sisotool. Çelik and Öztürk [46] presented one of the earliest applications of the Symbiotic Organisms Search (SOS) algorithm for optimizing proportional–integral (PI) controller parameters in DSP-based DC motor systems, demonstrating notable improvements in dynamic performance. Building on the idea of metaheuristic optimization, another study proposed a PI + derivative filter (DF) controller tuned via the stochastic fractal search technique, yielding enhanced speed regulation and robustness against disturbances [47]. More recently, nonlinear PI control strategies have been explored to further improve speed control characteristics of permanent magnet DC (PMDC) motor drives, emphasizing nonlinearities and practical implementation issues [48]. Complementary to these works, Çelik and Öztürk (2017) investigated SOS-based PI parameter tuning for DC motor drivers in a Turkish-language study, reinforcing the applicability of metaheuristics to classical control structures [49].

Using a PI controller for the speed regulation of the BLDC motors is not new. Tariq et al. [50] employed an Anti-Windup PI controller (AW-PIC) in a BLDC motor. Simulation results were validated by experiments on the motor with AW-PI through a Texas Instruments DSP board. Verma et al. [51] utilized a hybrid PI controller with fuzzy control in a series or parallel arrangement to regulate the speed of a Permanent Magnet Brushless DC (PMBLDC) motor. They used these two configurations in order to utilize the benefits of reduced motor output oscillations, fast operation, online parameter tuning, and enhanced robustness. Some other recent studies focused on optimization methods to adjust the PI controller gain parameters for the BLDC motor response control [52–60]. A most recent study by Sandip et al. [61] proposed a PSO algorithm-based PI controller for the BLDC motor. The PSO algorithm was used in a MATLAB/Simulink environment to tune the K_p and K_i gains for efficiently maintaining the necessary response speed of the motor under varying loads.

Some studies are found that investigated the tuning optimization of the PI controller used in DC servo motors. For instance, Sarkar et al. [62] used the method of time moments in order to estimate the controller parameters and speed regulation of a Permanent Magnet DC (PMDC) servo motor. They used the same technique to design the PI controller in a physical DC servo motor for the experimental validation of the simulation estimations. Both results had good agreement. Hote et al. [63] proposed a PI controller design based on Model Order Reduction (MOR) via the Gerschgorin theorem and singular perturbation technique. They conducted simulations as well as experiments and found that their results were in good agreement. Rai et al. [64] recently proposed a LabVIEW-based fuzzy PI controller model using a system identification method to achieve a real-time speed regulation of a DC servo motor. The simulation produced promising results.

Recent studies also explored artificial intelligence techniques for performance enhancement in DC servo motors. Fayad et al. [65] compared the performance of different controllers, such as conventional PID, FLC, and fuzzy with PID controller for the speed and position control of a DC servo motor under varying loads. In addition, they conducted experiments for the speed control of the DC servo motor using a PID controller. From the theoretical results, it was found that the fuzzy PI controller outperformed the other controllers in terms of overshoot and settling time. Mohamed et al. [66] employed adaptive neuro-fuzzy inference systems and Fuzzy FOPID control to enhance hybrid energy system performance, highlighting the potential of intelligent control in motor drive applications.

After a thorough literature review, it is revealed that most efforts have concentrated either on simulation-based tuning of PI controllers using metaheuristics, reinforcement learning strategies, nonlinear controller designs, or AI techniques, with limited focus on direct experimental validation of PI-based models for DC servo motors under varying load conditions. The novelty of the present work lies in bridging this gap by proposing a PI controller-based nonlinear model for the speed control of a DC servo motor, validated through a direct comparison of experimental and simulation results. Furthermore, unlike prior works that rely primarily on algorithmic optimization techniques, the current study also employs experiments and MATLAB Simulink model-based PID tuning algorithms to investigate the effects of P and I controllers on the error, damping, and stability of both the steady-state and transient motor response. Finally, optimized proportional and integral gains are obtained, providing practically implementable guidelines for optimum servo motor performance.

2. Material and methods

2.1. Angular velocity control

The velocity control servo system with feedback controller is shown in Fig. 1. The feedback controller has dual purpose; firstly, to bring the output speed y_ω in accordance with the set/established (reference) speed y_r by reducing the steady-state error to a minimum and secondly, to let the dynamic response of

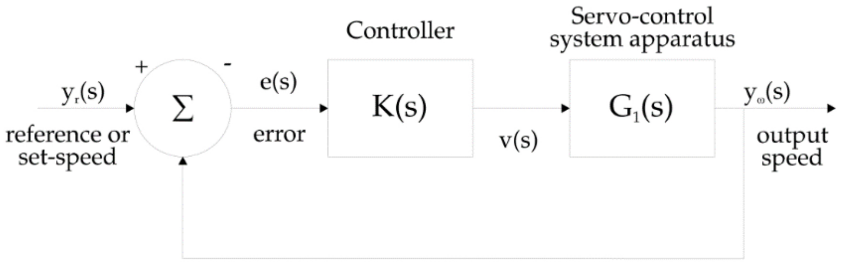

Fig. 1. Block diagram for velocity control servo system (reproduced with permission from TecQuipment Ltd.) [67].

the servo system vary according to the changes in the reference speed.

2.2. Steady-state error

For a constant reference speed y_r, the general expression of the steady-state error e_{ss} for the servo system, shown in Fig. 1, in the frequency domain can be expressed as [67]

$$e_{ss} = \lim_{s\to 0}\left[\frac{y_r}{1 + K(s).G_1(s)}\right] \tag{1}$$

where $K(s)$ is the controller transfer function, $G_1(s)$ is the servo system transfer function, and y_r is the potentiometer reference speed signal. If both proportional and integral controls are used in the servo system transfer function, then $K(s)$ can be written as [67]

$$K(s) = K_p + \frac{K_i}{s} \tag{2}$$

Substituting it in (Eq. (1)) yields [67]

$$e_{ss} = \lim_{s\to 0}\left[\frac{s.y_r}{s + \left(K_p.s + K_i\right).G_1(s)}\right] \tag{3}$$

The steady-state error e_{ss} is inversely proportional to the proportional and integral gains K_p and K_i, respectively. With the use of both controllers in the transfer function, e_{ss} is expected to be zero.

2.3. Dynamic response

The influence of the feedback loop on the dynamic response of the speed control servo system can be analyzed with the help of the closed-loop transfer function given as [67]

$$y_\omega(s) = \frac{K(s)\,G_1(s)\,y_r(s)}{1 + K(s)\,G_1(s)} \tag{4}$$

where y_ω is the output voltage proportional to the angular velocity of the shaft ω. The speed transfer function $G_1(s)$ is a second order transfer function. However, considering the servo-control system alone, it has an inertial load and assuming the inductance of the armature to be small compared with the inertia of the flywheel, it is reduced to first order transfer function given as [67],

$$G_1(s) = \frac{G_1}{Ts + 1} \tag{5}$$

where G_1 is the gain of the speed transfer function or motor gain, and T is the closed-loop time constant. With the P and I controllers considered in the feedback controller, substituting the expressions for $K(s)$ from (Eq. (2)) and $G_1(s)$ from (Eq. (5)), the transfer function of (Eq. (4)) becomes

$$y_\omega(s) = \left[\frac{\left(K_i + K_p.s\right)G_1}{Ts^2 + \left(1 + K_pG_1\right)s + K_iG_1}\right] y_r(s) \tag{6}$$

The closed-loop transfer function of the speed control servo system with P and I controllers (Eq. (6)) is of second-order. Therefore, it can be compared with the general expression of a second-order transfer function [67].

$$y(s) = \frac{\omega_n^2}{s^2 + 2\xi\omega_n s + \omega_n^2} y_r(s) \tag{7}$$

where ξ is the damping ratio and ω_n is the system's natural frequency. Comparing the denominators of (Eqs. (6) and (7)) yields the expressions for ξ and ω_n in terms of the transfer function gain G_1 and the time constant T.

$$\omega_n^2 = \frac{K_iG_1}{T} \tag{8}$$

$$2\xi\omega_n = \frac{1 + K_pG_1}{T} \tag{9}$$

From (Eqs. (8) and (9)), the desired improvement in the closed-loop dynamic response of the velocity control servo system can be achieved with the help of

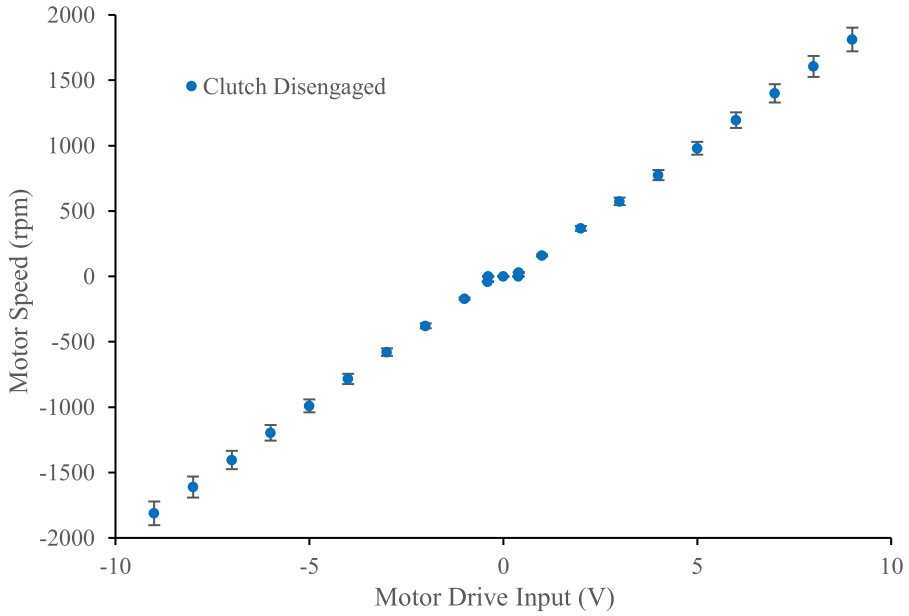

Fig. 2. Motor calibration curve.

suitable values of ω_n and ξ obtained through careful selection of K_p and K_i values.

2.4. Experiment

2.4.1. Equipment

The equipment used in the current experiments to regulate the speed of the DC servo motor through a PI controller is the TecQuipment servo trainer apparatus (TQ CE110), a TecQuipment analog PID controller (TQ CE120), and an interfaced computer. These are the same equipment used by Bahakeem and Jamal [68]. TQ CE110 is designed to control the speed and the angular position of the DC servo motor via a PID controller. The DC servo motor operating parameters include an electrical supply of 50/60 Hz with earth, 220 V to 240 V with 0.5 A current, operating temperature range of $+5^{\circ}$C to $+40^{\circ}$C, and operating relative humidity range of 80% at temperatures $< 31^{\circ}$C that linearly decrease to 50% at 40°C. A DC servo motor, a DC generator, a flywheel, an electrically operated clutch system, and a 30:1 reduction gearbox assembly are embedded in this apparatus. The clutch system and the gearbox assembly are utilized in controlling the angular position of the DC servo motor. An analog input signal to the motor circuit in the range of 1 to ± 10 V enables the motor to rotate in either direction with an angular velocity of up to 1999 rpm, which is optically sensed and displayed on the digital readout screen. Additional inertial loads in the form of removable circular discs can be added to the common shaft housing the permanently fixed flywheel. The analog controller TQ CE120 is connected to the TQ CE110 trainer for the DC motor speed regulation. It comprises a signal generator to generate a steady-state, step, or other input signal forms, Proportional (P), Integral (I), and Derivative (D) controllers, and other accessories to build closed-loop or open-loop control circuits. The computer connected with the equipment has a compatible CE 2000 software that is used for data input, output data analysis, and data storage.

2.4.2. Motor calibration

The circuit of the actuator (the motor circuit) is calibrated. The servo trainer is connected to analog controller. As part of first set-up, the clutch is disengaged, i.e., position shaft is not connected and potentiometer knob position is set at the center showing a reading of 0 V. The potentiometer voltage is increased by turning the potentiometer control clockwise until the motor just starts to turn. This is called the positive dead-zone for motor amplifier. The voltage is increased to 10 V in steps of 1 V and the corresponding motor speed from the speed display on the CE110 front panel is recorded. Then, the procedure is repeated with negative voltage. Fig. 2 shows the corresponding calibration curve.

From the experimental results, a linear correlation is established between the motor speed and the motor drive input through the equation

$$\omega = 199.29v - 2.8261 \tag{10}$$

From Fig. 2, the slope of the linear regression gives the motor drive sensitivity as $k_i = 199.29$ rpm/volts

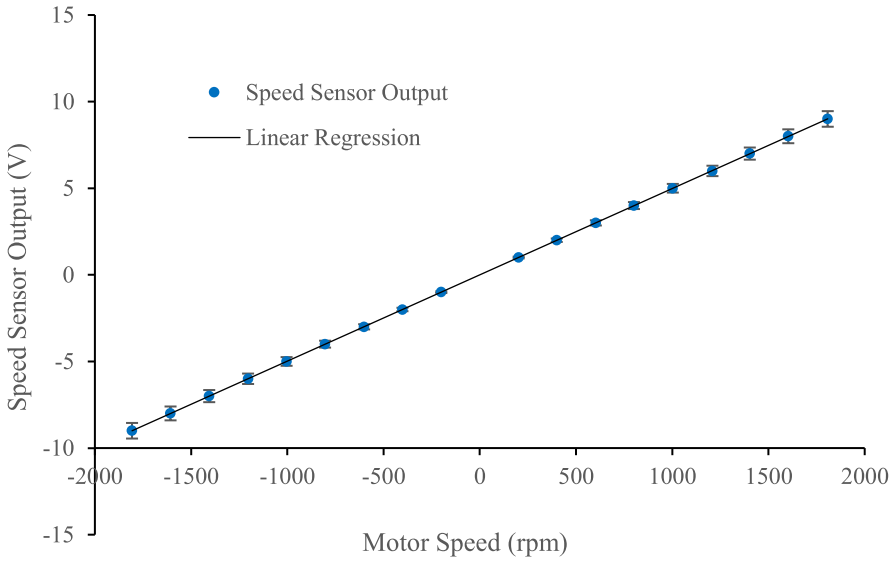

Fig. 3. Speed sensor calibration.

2.4.3. Speed sensor calibration

The output speed sensor is calibrated. The clutch is disengaged and potentiometer knob position is set at the center showing a reading of 0 V. The potentiometer voltage is slowly increased by turning the potentiometer control clockwise until the speed sensor reads 1 V. The voltage is increased to 9 V in steps of 1 V and the corresponding motor speed from the speed display on the CE110 front panel is recorded. The process is repeated in steps of 1 V for positive and negative speed sensor reading in the range of -9 V to +9 V. Fig. 3 shows the corresponding calibration curve.

A linear correlation, thus obtained, between the speed sensor output and motor speed is given as,

$$y_\omega = 0.005\omega + 0.0008 \tag{11}$$

From Fig. 3 the slope of the linear regression gives the speed sensor sensitivity as $k_\omega = 0.005$ volts/rpm.

The error bars in Figs. 2 and 3 show the experimental readings accuracy error of 5%, which is a commonly anticipated value. In this view, the measurement precision or confidence level is 95%. This reading accuracy error could be because of inaccurate measurement of positive and negative dead-zones and recording the average values of the slightly oscillating motor drive speeds from the speed display on the CE110 front panel.

2.4.4. Experimental set-up

In the present set of experiments, TQ CE110 is connected to TQ CE120 and the computer. Initial control settings of CE110 are obtained by engaging only P and I controllers, disengaging the clutch system, installing both the circular discs on the flywheel shaft, and firmly closing the rear access door of the servo trainer. The load thus applied to the apparatus due to the two installed discs is referred to as the largest inertial load. Derivative (D) controller is not included in the light of experimental theoretical results reported in Section 3.1. Therefore, the theoretical model formulated in Sections 2.2 and 2.3 for the present study involves only P and I controllers. The electrical connections between the servo trainer and the analog controller are shown in Fig. 4.

2.5. Simulation

In a MATLAB Simulink environment, the DC motor's theoretical response via the second-order speed transfer function is determined. The given values of PI controller gains K_p and K_i, without K_d, are fed into (Eq. (6)). The motor gain $G_1 = 1.0059$ and the time constant $T = 1.60$ sec. for the largest inertial load, obtained experimentally by Bahakeem and Jamal [68], are also substituted in (Eq. (6)). The transfer function after substitution can be written as

$$y_\omega(s) = \left[\frac{\left(K_i + K_p.s\right)1.0059}{1.60s^2 + \left(1 + 1.0059K_p\right)s + 1.0059K_i}\right] y_r(s) \tag{12}$$

The detailed derivation of (Eq. (12)) can be seen in Appendix 1.

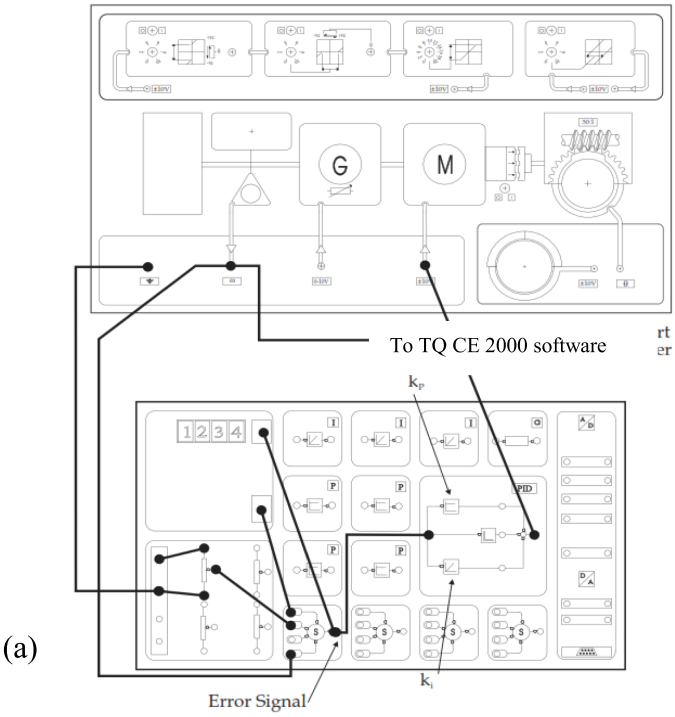

(a)



(b)

Fig. 4. (a) Schematic diagram and (b) actual photo of Electrical connectivity of TQ CE110 and TQ CE120 (reproduced with permission from TecQuipment Ltd.) [67].

3. Results and discussion

The current section accounts for studying the effects of the I and P controllers on the DC motor response subjected to steady-state and step input signals, calculating the K_p and K_i values at given system undamped natural frequency ω_n and damping ratio ξ for specific unsteady (transient) response of the DC motor, and obtaining the optimized values of K_p and K_i for an effective DC servo motor speed response. The steady-state and transient responses of the motor are obtained via experiments and compared with the theoretically obtained responses whereas the controller parameters optimization is done theoretically in the MATLAB Simulink environment. The response performance parameters, such as the peak time, rise time, and overshoot, are obtained experimentally and theoretically, and then compared. Another important

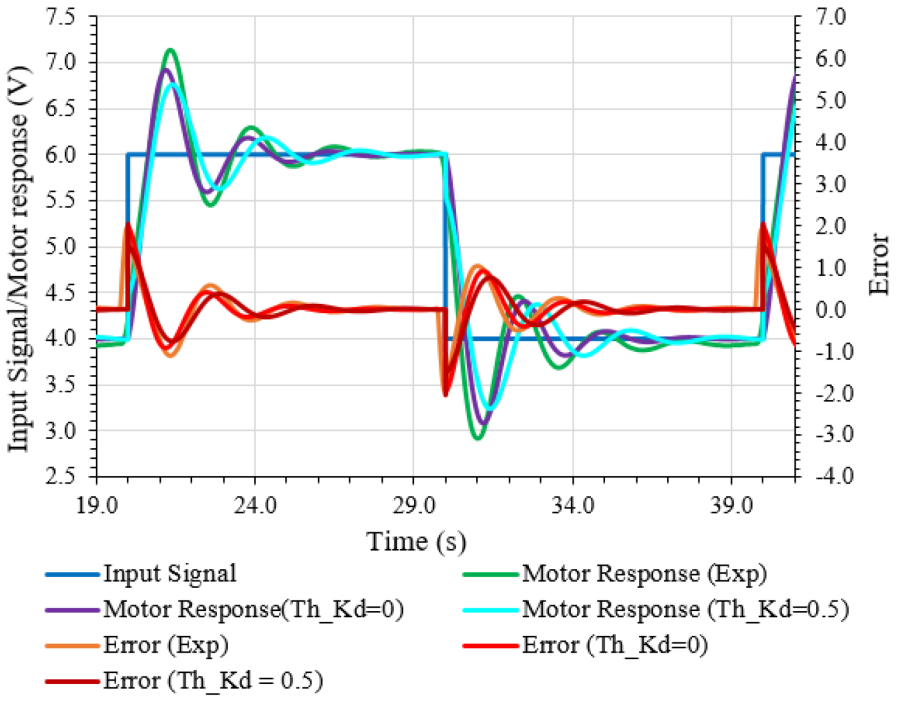

Fig. 5. Motor response obtained experimentally and theoretically at two values of K_d.

analysis pertinent to the effect of load disturbances on motor performance is addressed in another work by Bahakeem and Jamal [68].

3.1. Derivative (D) controller

A special case is run theoretically and compared with the experimental results without the D controller to determine the efficacy of the D controller in motor speed control. The experimental set-up without the D controller is conducted with the set-up mentioned in Section 3.1. The potentiometer is set to 5 V, and an input square wave of frequency 0.05 Hz is generated with a level of 1 V and zero offset. The controller gains K_p and K_i are set at values 1 and 10, respectively. The response of the DC servo motor is recorded for a time span of 50 seconds. Then, the theoretical runs are completed with the same values of K_p and K_i using Simulink toolbox with different values of derivative gain K_d. The experimental and theoretical transient responses are plotted together to see if the D controller contributes significantly to the motor speed control. Fig. 5 shows the plot of step input signal and motor experimental and theoretical response in volts versus time for $K_d = 0$ and 0.5. Comparing the theoretical response performance parameters of the servo system with ($K_d = 0.5$) and without the D controller ($K_d = 0$), it is observed that the D controller causes a 15.70 % and 42.89 % increase in the peak time and rise time, respectively, and 19.35 % decrease in the overshoot. In addition, it also causes a 6.67 % and 29.84 % decrease in peak time and overshoot, respectively, and 14.40 % increase in rise time when compared with the experimental results of the DC motor response.

Fig. 6 results, obtained using the Simulink toolbox, compare the motor response with K_d ranging from 0 to 5. This figure is complemented with Fig. 7 to observe the system performance with K_d. The system performance parameters, such as the rise time, overshoot, and peak time, are considered to assess the system response. Rise time is the time necessary for a system's reaction to increase from 10% to 90% of its steady-state value. Overshoot is the percent difference between the first instantaneous peak response and the steady state. Peak time is the time needed by the system to reach the first instantaneous peak response. These performance parameters are obtained through a MATLAB code in which the standard syntax "stepinfo (y, t, y_{final})" is used to find these parameters. It is observed in both figures that initially, an increase in K_d does not cause a significant improvement in the results in terms of peak time and rise time. However, the overshoot decreases minimally with K_d. As K_d increases beyond 0.5, the controller causes the motor to respond abruptly to the step input function. This abrupt response becomes more severe at higher values. Such a type of response in a physical system can damage the motor. The typical characteristics of the D controller can be observed in

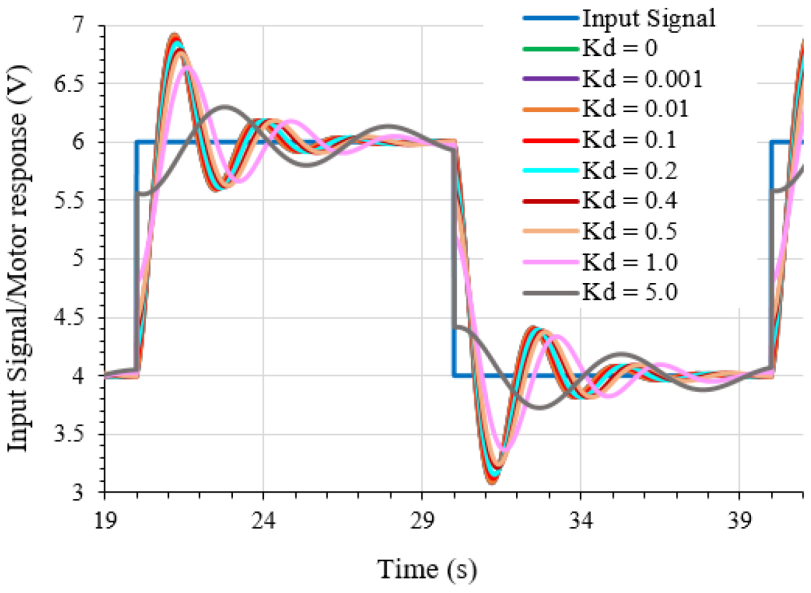

Fig. 6. Motor response obtained theoretically at different values of K_d.

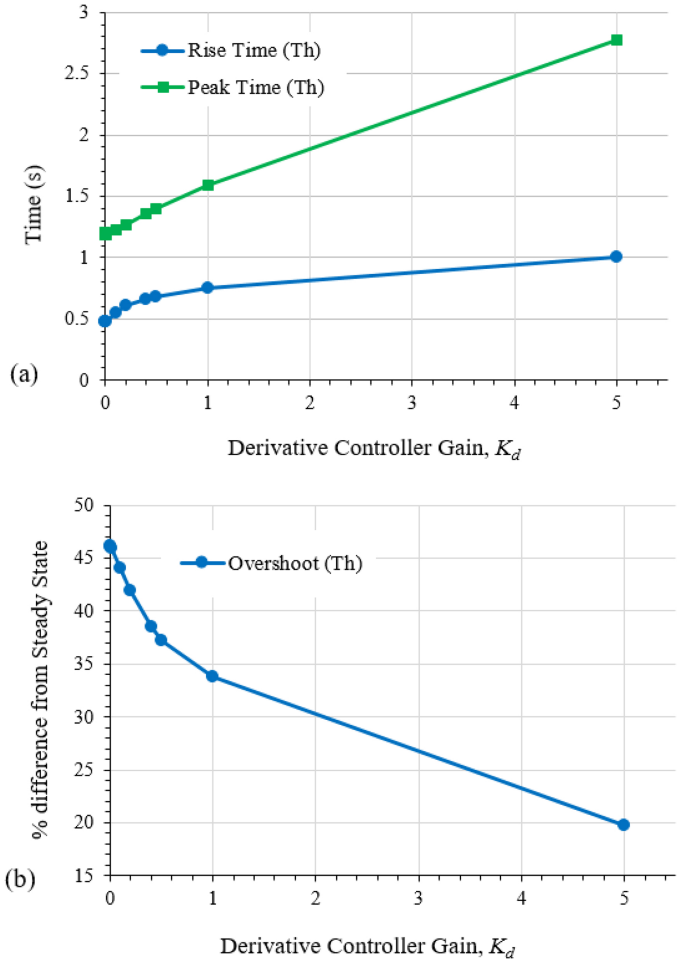

Fig. 7. Variation of transient response performance parameters (a) rise time and peak time, and (b) overshoot with K_d.

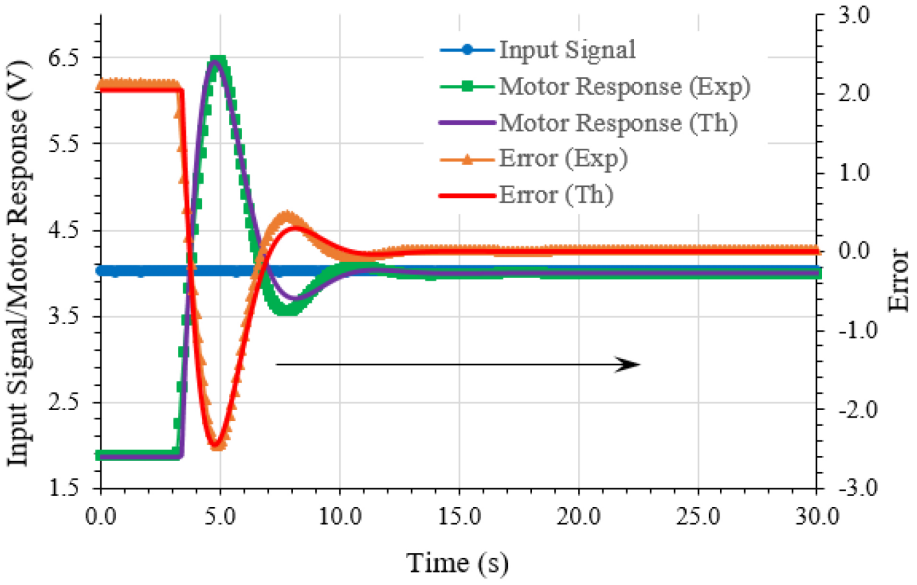

Fig. 8. Motor steady-state response obtained experimentally and theoretically with $K_i = 2$.

the figures. Higher gain values of the controller do not eliminate the steady-state error. Also, an increase in K_d increases the response time, as can be seen in the figures below. All these factors, with the abrupt change in the response, make the D controller not suitable for the DC motor speed regulation in the present work. Therefore, the effects of only P and I controllers are currently explored.

3.2. Steady-state results

3.2.1. Effect of I controller

The experimental results are obtained using the same set-up mentioned in Section 3.1. Proportional gain K_p is set to 1. Function generator offset is set to zero, and the DC level zero. Potentiometer voltage is initially zero, which is gradually increased to 4 V. The integrator reset button is pressed before switching in the I controller into the circuit. Initially, $K_i = 0.1$ is set, and the experiment is run. The data is plotted and stored in the computer through the compatible software CE 2000. Then the experiment is repeated for the values of $K_i = 0.5$, 1, 2, 4, 6, and 10, and the data for each value is stored. The speed transfer function with the proportional and integral controller modules is fed into the Simulink toolbox and run for the same values of K_i. The response for each K_i thus obtained is then plotted with the corresponding experimental response. Here, only representative results are presented due to space constraints. Fig. 8 shows the motor response in terms of volts obtained theoretically and experimentally with time for $K_i = 2$. The error representing the difference between the process variable, in the present case, is the motor angular velocity read as output voltage, and the steady-state input signal or set point is plotted on the right-hand side secondary axis. It is observed in the figure that K_i eliminates the steady-state error, but at the same time decreases the speed of system response as expected through the introduction of more oscillations before reaching the steady-state. These oscillations become more pronounced at higher values of K_i, which can further lead to unbounded oscillations. Thus, it can be stated that the system stability has reduced. This outcome can be clarified by the fact that with the introduction of the I controller, an additional pole is added to the system. That increases the order of the system, and it becomes more unstable. Comparing the experimental and theoretical responses of the system shows good agreement.

Fig. 9 shows the rise times and the peak times extracted from the experimental and theoretical system responses of Fig. 8. Here, these response performance parameters are obtained for K_i values 1, 2, 4, 6, and 10. It is observed that the rise time and the peak time decrease with K_i. Here, just considering the effect of the I controller, it is known that the integral controller output is directly proportional to the time integral of the error given as.

$$I(t) = K_i \int_0^t e(t)\, dt \tag{13}$$

where $I(t)$ is the system output due to the integral controller output, and $e(t)$ is the time-dependent error signal. With K_i, the system output produces a larger error signal, and in order to achieve zero error, the output ramps up, or in other words, the output

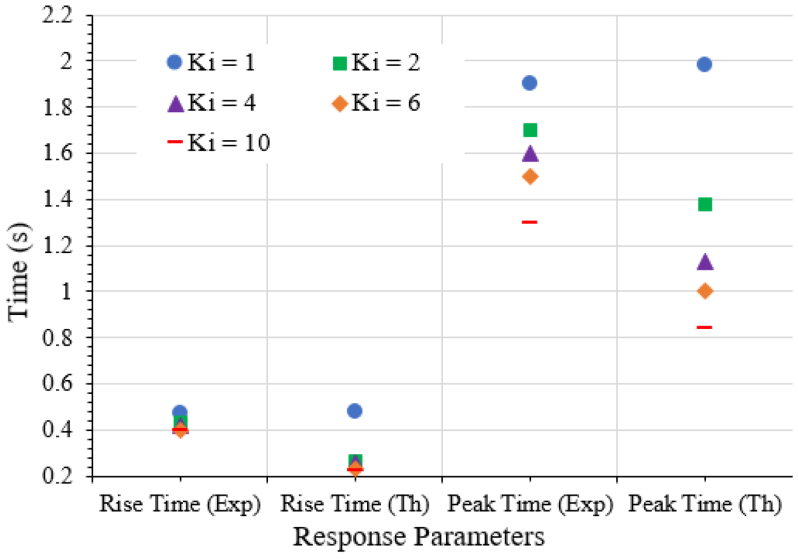

Fig. 9. Variation of steady-state response performance parameters with K_i.

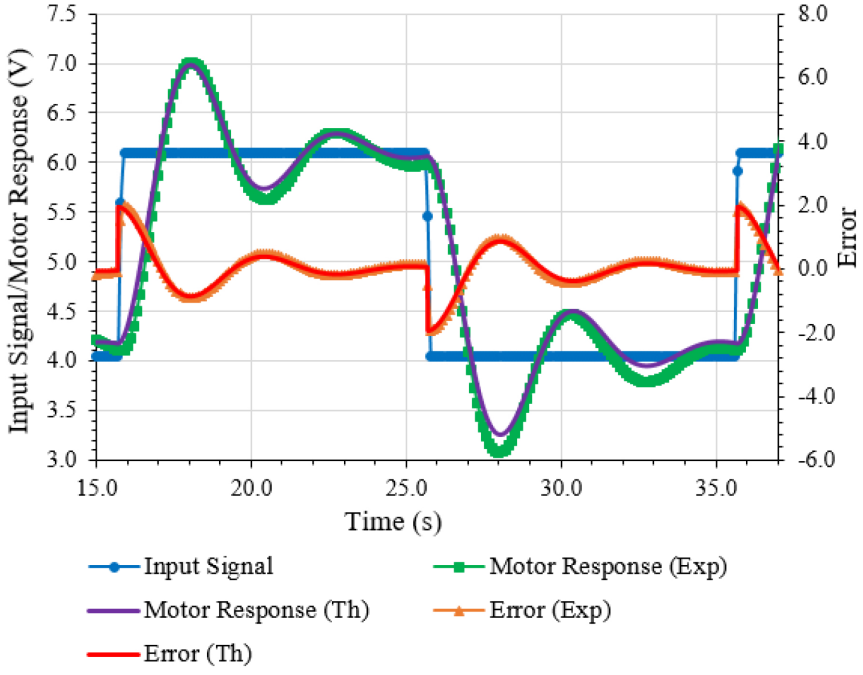

Fig. 10. Motor transient response obtained experimentally and theoretically with $K_p = 0.1$.

derivative increases, resulting in reduced rise time and peak time.

3.3. Transient results

In this section, the unsteady (transient) response of the DC motor influenced by the P and I controllers is investigated. The electrical connections are made according to Fig. 4, and the experimental set-up is the same as indicated in Section 3.1. The potentiometer is set to 5 V ± 1 V, and an input square wave of frequency 0.05 Hz is generated with zero offset. The theoretical results are obtained via the MATLAB Simulink toolbox.

3.3.1. Effect of P controller

First, the influence of the P controller on the motor response is investigated experimentally and theoretically. In this case, the integral gain K_i is set at a constant value of 3, while three distinct values of

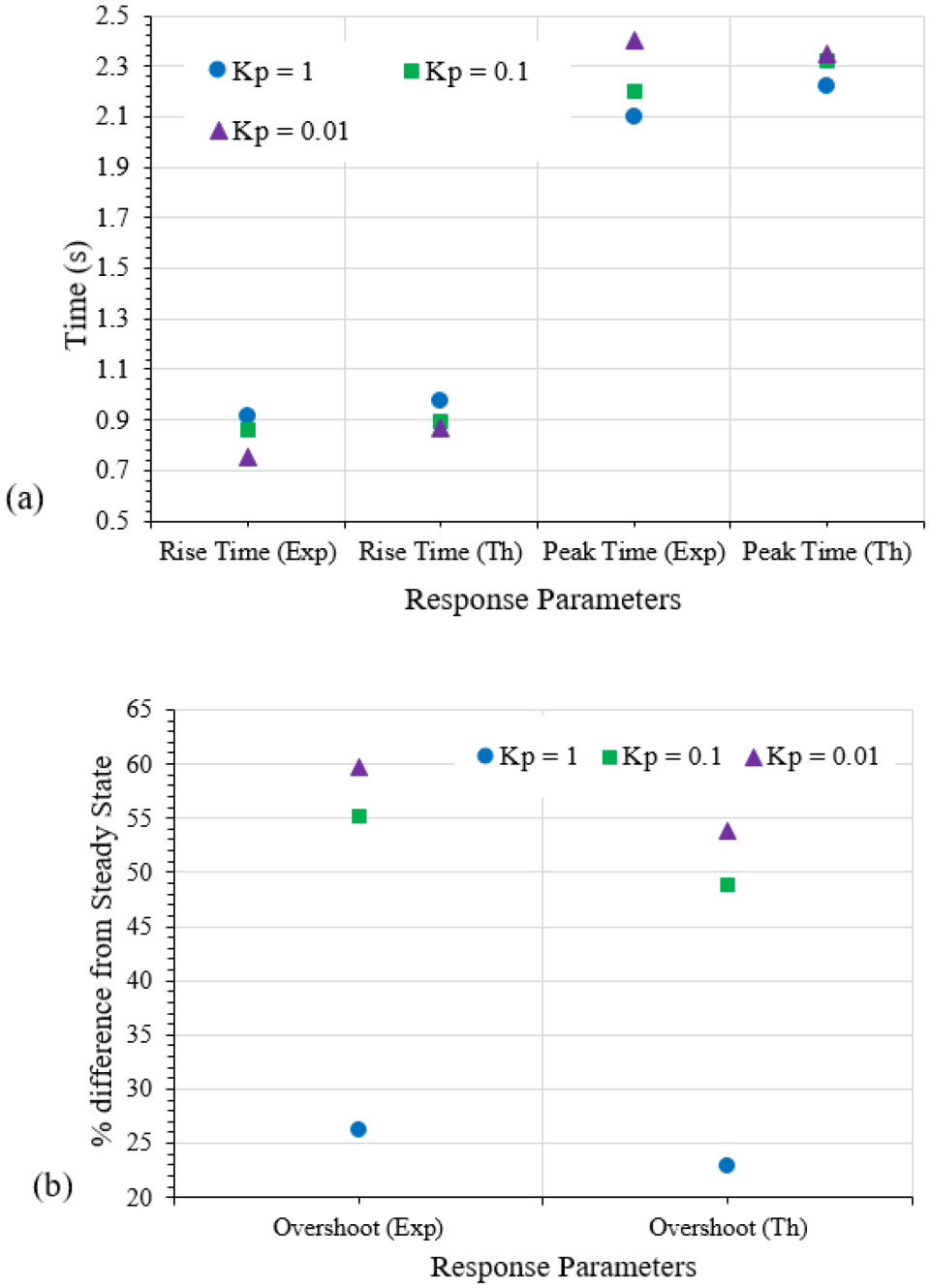

Fig. 11. Variation of transient response performance parameters (a) rise time and peak time, and (b) overshoot with K_p.

the proportional gain K_p (1, 0.1, and 0.01) are used for the response. The rationale behind choosing the values of K_p is to avoid complete dominance of P controller at high values of K_p since the present work intends to utilize the strengths of both P and I controllers for the speed control system. In addition, the values of K_p are within the range of CE120 analog controller. As can be seen in Fig. 10 for $K_p = 0.1$, the agreement between the experimental and theoretical responses is very good. In addition, it is also observed that as K_p decreases, the concurrency of the two results deteriorates slightly. The reason is that with the decline of K_p, the response oscillations magnify, and due to the inherent inertia of the physical system, i.e., the motor, the decay of oscillations slows down. No inertial term is present in the theoretical model; therefore, such a delay in the oscillation decay is not observed, resulting in a slight discrepancy in the results. In addition, it is also observed that as the K_p decreases, the system damping decreases and the

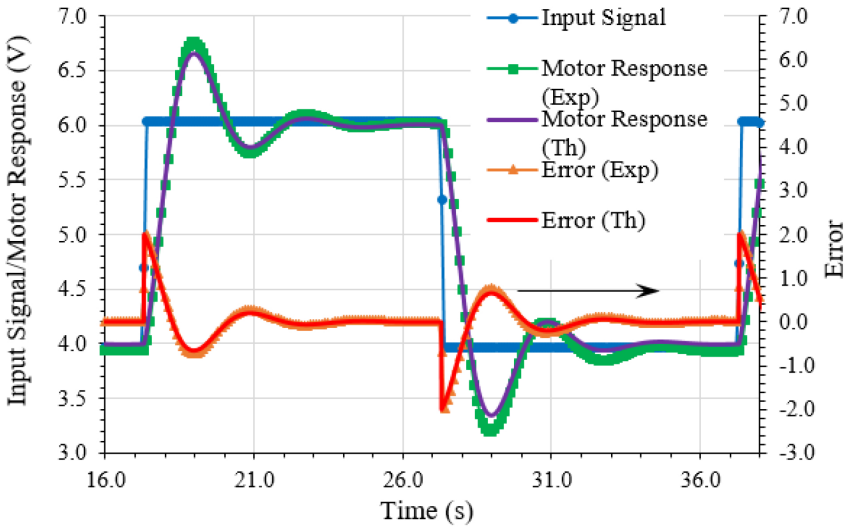

Fig. 12. Motor transient response obtained experimentally and theoretically with $K_i = 5$.

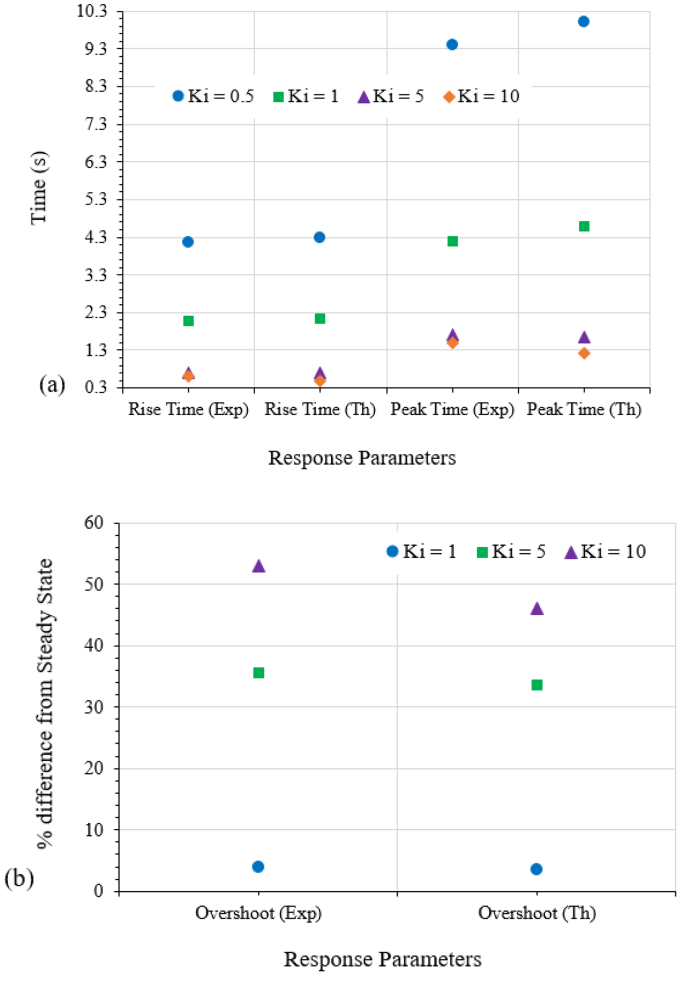

Fig. 13. Variation of transient response performance parameters (a) rise time and peak time, and (b) overshoot with K_i.

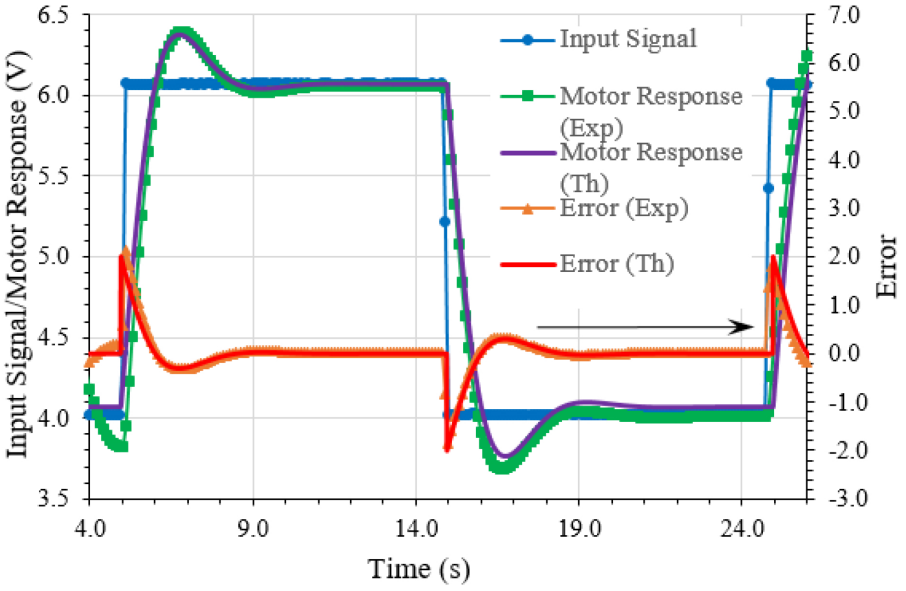

Fig. 14. Motor transient response obtained experimentally and theoretically with damping ratio $\xi = 0.6$.

influence of K_i becomes more profound resulting in an increase in the maximum overshoot. In addition to this, it can be inferred that if K_p is further reduced, it can lead to the deterioration of system stability evident from the increased overshoot and delayed response at smaller values of K_p. However, the natural frequency of response does not change. This, in turn, delays system response to achieve a steady state response.

Fig. 11 shows the experimental and theoretical system response performance parameters for the given values of K_p. It is observed in Fig. 11a that with a decrease in K_p, the rise time has slightly decreased. As a result of the P controller, the rise time should increase with a decrease in the P controller gain. The reason is that at a given smaller value of K_p, the integral controller gain ($K_i = 3$) becomes dominant and its capability to decrease the rise time prevails. The net result of these opposing effects is a slight decrease in the rise time. The peak time increases with a decrease in K_p because of the inherent effect of the P controller and the dominant effect of the I controller, which increases the maximum overshoot of the system response, as shown in Fig. 11b. This behavior is the characteristics of a system with small and large values of proportional and integral gains, respectively, and is expected in the results. Fig. 11b shows an increase in the maximum overshoot with decreasing K_p. This system response trend is an inherent characteristic of very small K_p and relatively large dominant K_i.

3.3.2. Effect of I controller

This section investigates the effect of the integral controller on the servo motor response obtained experimentally and theoretically. Values of $K_i = 0.5$, 1, 5, and 10 are employed. $K_p = 1$ is kept constant. It is worth mentioning that very smaller values of K_i are not considered to avoid complete dominance of K_p at such values of K_i. Moreover, CE 120 analog controller imposes a limit on the range of K_i values to be considered for the analysis. Representative results are presented here in Fig. 12 for $K_i = 5$. At small value of $K_i = 0.5$, the servo motor shows no overshoot because of a very small value of K_i. However, the overshoot because of the oscillations in the response starts to appear for K_i =1. This effect becomes more pronounced at larger values of K_i, such as 5 and 10. By increasing K_i, one of the advantages of the integral controller is achieved, which is that the steady-state error is eliminated. But at the same time, system stability in terms of the magnitude and longer prevalence of the oscillations, the damping, and the speed of response are also affected. It is also clear from the figures that as the integral controller gain K_i increases, the system response to the produced error in the form of the overshoot becomes slower due to the generation of more response oscillations.

Fig. 13(a,b) shows the rise times, peak times, and overshoots of the experimental and theoretical system responses with increasing K_i. The integral gain of 0.5 does not produce considerable deviation from the input signal, resulting in no overshoot. Therefore, it is not included in the plot of overshoot (Fig. 13(b)). Fig. 13(a) shows the characteristics of K_i, i.e., it reduces both the rise time and peak time. However, the maximum overshoot or the initial maximum error increases with K_i as can be seen in Fig. 13(b).

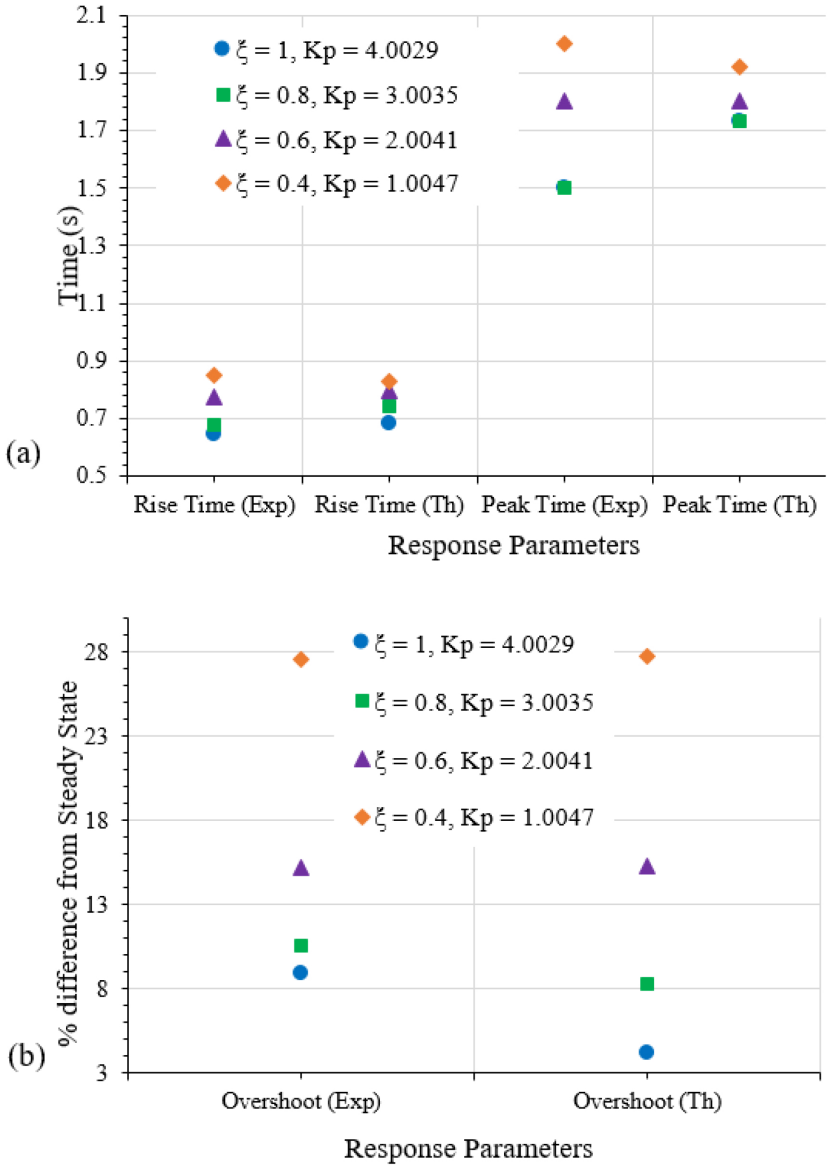

Fig. 15. Variation of transient response performance parameters (a) rise time and peak time, and (b) overshoot with different values of damping ratio ξ.

3.3.3. Damping ratio

The current section presents an account of the influence of the P controller on the system's closed-loop transient response at a desired undamped natural frequency $f_n = 0.25$ Hz of the system response. The frequency is converted to $\omega_n = 1.5708$ rad/sec by applying the conversion expression $\omega_n = 2\pi f_n$. The same experimental set-up described in Section 3.1 is kept for this analysis. It is known that with a decrease of P controller gain, the damping ratio ξ decreases and the system response, in response to any imposed perturbations, will take a longer time to damp out the overshoot or oscillations. This can be mathematically understood with the help of the standard expression,

$$K_p = \frac{2\xi\omega_n T - 1}{G_1} \tag{14}$$

It is clear from the expression that any reduction in K_p results in a decrease in the damping ratio. On the contrary, K_i does not influence the damping ratio, as shown in the expression,

$$K_i = \frac{T\omega_n^2}{G_1} \tag{15}$$

Here, the K_p is reduced in a different manner. Instead of using different reducing values the K_p to

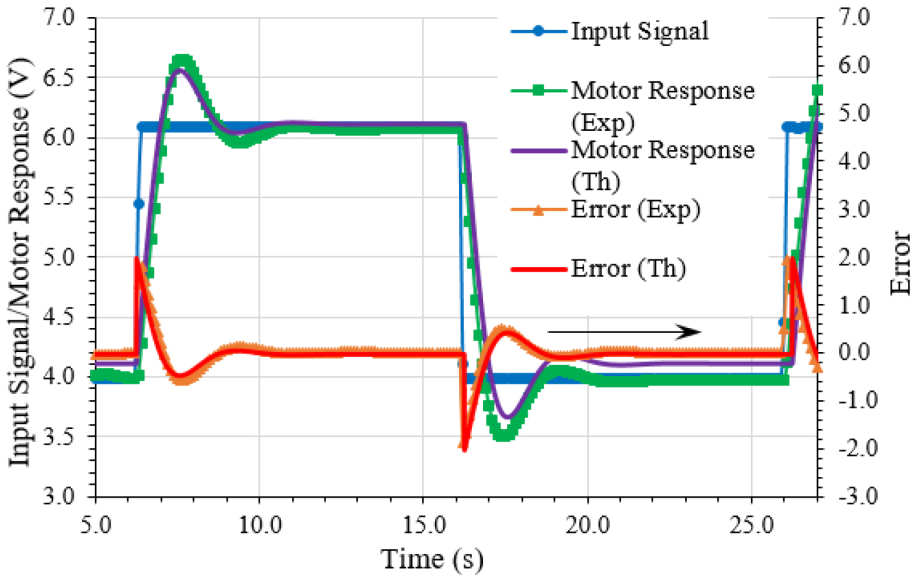

Fig. 16. Motor transient response obtained experimentally and theoretically with the desired natural frequency, $\omega_n = 2.0944$.

obtain ξ from the above expression, desired values of $\xi = 1$, 0.8, 0.6, and 0.4 are used to obtain the values of K_p from (Eq. (14)) $K_p = 4.0029$, 3.0035, 2.0041, and 1.0047, respectively. Since K_i is not a function of ξ, as can be seen in (Eq. (15)), a constant value of it ($K_i = 3.9247$) is obtained for this analysis. Here, only representative results for $\xi = 0.6$ are presented. Fig. 14 shows the experimental and theoretical transient closed-loop responses of the system varying with the K_p. With the decrease in K_p, the damping ratio ξ, which is an indicator of the inherent damping of the system, decreases, affecting the response amplitude and the time to stabilize the system, or in other words, bring the system to the required set value. However, the frequency of response does not change.

Fig. 14 depicts the experimental and theoretical closed-loop system response performance parameters varying with decreasing K_p. These parameters are obtained both experimentally and theoretically. As mentioned above, at a given natural frequency, a decrease in K_p decreases the damping ratio that, in turn, increases the rise time and peak time as shown in Fig. 15(a). On the other hand, the overshoot also increases with a decline in K_p or ξ, shown in Fig. 15(b).

3.3.4. Response frequency

In this section, the system's transient response at desired undamped natural frequencies (speed of response) $f_n = 0.5$, 0.33, 0.25, and 0.2 Hz, is investigated at a given fixed damping ratio $\xi = 0.5$. The frequencies (f_n) are converted to $\omega_n = 3.1416$, 2.0944, 1.5708, and 1.2566 rad/sec. Here, the desired values of ω_n and ξ define the values of K_p and K_i through (Eqs. (14) and (15)), respectively. The values thus obtained are $K_p = 4.0029$, 2.3372, 1.5044, and 1.0047, and $K_i = 15.6987$, 6.9772, 3.9247, and 2.5118. To run the experiment at these values of K_p and K_i, it is observed that the value of integral gain (K_i =15.6987) is higher than the highest value for K_i that can be set in the CE120 analog controller. Therefore, the first set of values of K_p and K_i are not run experimentally on the CE110 servo trainer. Fig. 16 shows the representative experimental and theoretical motor responses at two different desired natural frequency $\omega_n = 2.0944$. The corresponding value of K_p is 2.3372 and K_i is 6.9772. Note that the motor response corresponds approximately to the expected standard second-order system response.

Fig. 17(a) and Fig. 17(b) show the experimentally and theoretically derived rise time, peak time, and overshoot as they change with the intended natural frequency of the system response (ω_n), the proportional controller gain (K_p), and the integral controller gain (K_i). It is observed that with a decrease in the undamped natural frequency ω_n at a given damping ratio ξ, both the controller gains K_p and K_i drop linearly and nonlinearly, respectively, resulting in an increase in the peak and rise times, whereas a decrease in the overshoot. It is clear from these results that reducing the response undamped natural frequency directly affects the system by inducing a delay in reaching its steady state or desired set value.

3.4. Optimization

A wide variety of optimization techniques are available to maximize the output efficiencies of systems generating power or controlling processes. One such

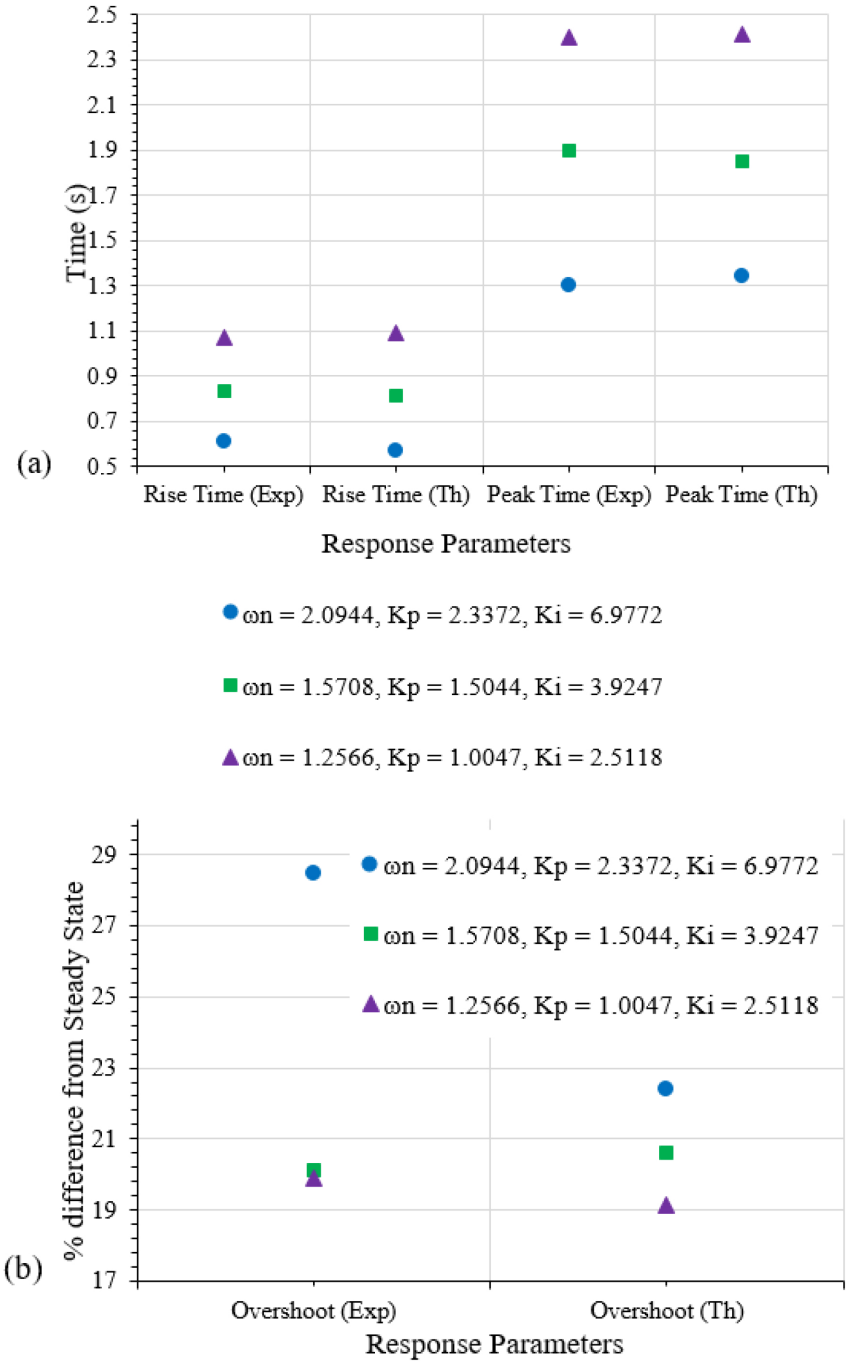

Fig. 17. Variation of transient response performance parameters (a) rise time and peak time, and (b) overshoot with the desired natural frequencies ω_n.

practical example is the utilization of two optimization techniques namely PSO and Electric Eel Foraging Optimization (EEFO) to enhance the PV and wind turbine hybrid system performance connected to a power grid [69]. Likewise, the PI controller performance is expected to enhance if optimized values of P and I controller gains are obtained through an optimization technique. This can enable the system to attain the enhanced P and I controller characteristics of rapid system response and reduced deviation from the set process variable. Therefore, optimized values of the controller gains are obtained in the present investigation.

The optimized values are determined in the MATLAB Simulink environment through a model-based PID tuning algorithm commonly called "Automated

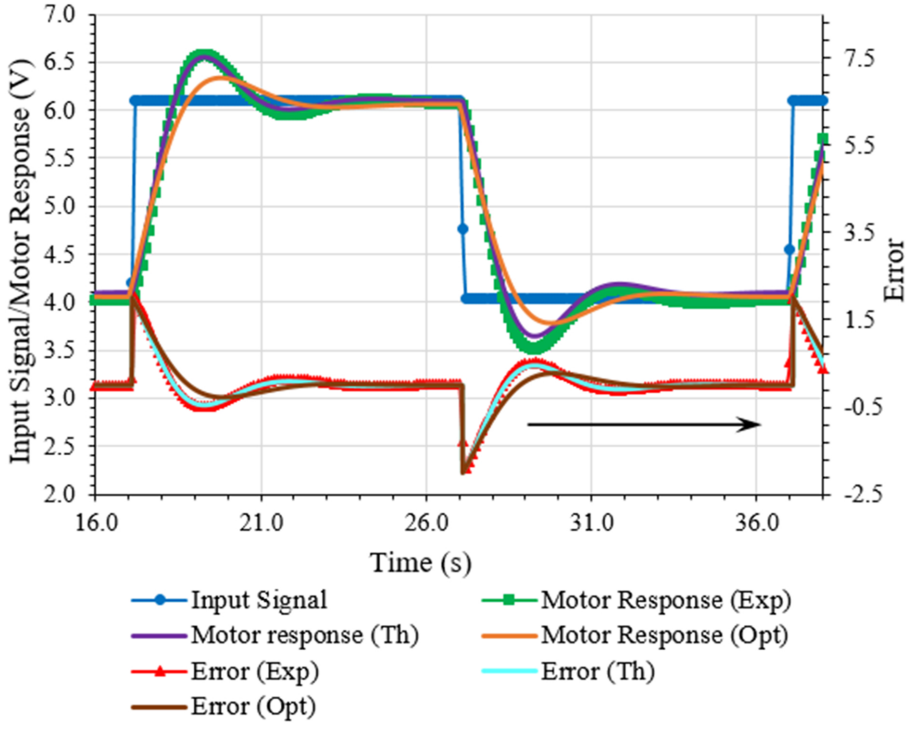

Fig. 18. Comparison of the experimental transient response of motor with $K_p = 1$ and $K_i = 3$ and the theoretical response with optimized values of $K_p = 1.0363$ and $K_i = 1.9438$.

tuning". This algorithm involves the following steps: (a) Model Linearization; MATLAB Simulink linearizes the model for optimization by approximating nonlinear systems with linear models around operating point, (b) Selection of Controller Type; Simulink uses numerous tools and methods to optimize selected controllers, concentrating on parameter tweaking rather than controller type, (c) Frequency-Domain Loop Shaping; Simulink adjusts the controllers approximating the intended loop shape for the response, (d) Automatic Gain Adjustment; Simulink optimizes control systems and signal processing using multiple automated gain adjustment algorithms. These strategies strive to ensure system performance, such as output consistency, stability, or response optimization, (e) Resulting Optimized Gains; the optimized values of the controller gains are obtained, and (f) Validation; MATLAB Simulink validates optimization findings using multiple approaches, especially for parameter estimates and design optimization. The validation procedure verifies that optimal parameters or design choices match system behavior or performance criteria.

With the PI controller block selected and given values of $K_p = 1$ and $K_i = 3$ entered in the Simulink toolbox, the simulation is run. Then the "Tune. . ." button is pressed to obtain the tuned or optimized values of K_p and K_i. The "Tune. . ." button enables the Simulink to follow the steps of optimization outlined above. The values thus obtained from this feature are $K_p = 1.0363$ and $K_i = 1.9438$. Fig. 18 shows the comparison of the system response obtained from the experiment and Simulink before (with $K_p = 1$ and $K_i = 3$) and after optimization. The optimized system exhibits more stability than that without optimized gain values marked by reduced overshoot. However, its peak time and rise time show an increase. At the same time, the settling time reduces, which means that the desired steady state or set point is achieved by the system earlier than the non-optimized system response. A quantitative comparison of the optimized and non-optimized performance parameters is presented in Table 1.

The currently obtained optimized values of K_p and K_i, and the optimized performance parameters are also compared with those through other optimization techniques such as PSO and FLC. Samat et al. [43] and Mansor et al. [42] obtained the optimized K_p and K_i values, and the corresponding performance parameters using PSO and FLC, respectively, for an unloaded DC motor working at a dynamic speed range of 1000-1500. Samat et al. [43] obtained the values of $K_p = 8.72$ and $K_i = 0.92$, whereas Mansor et al. [42] obtained both K_p and K_i values in the range of 0 to 1. Same parameters were also calculated by Samat et al. [43] for loaded DC motor condition. The values are shown in Table 2. Comparing these values with present work values show some discrepancy. It

Table 1. System response performance parameters of experimental and theoretical results obtained before and after optimization.

Response mode/Parameters	Rise Time (sec)	Peak Time (sec)	Settling Time (sec)	Overshoot (%)
Experiment	0.90492	2.10	6.01	26.17
Theory	0.97249	2.22	5.75	22.89
Theory (Optimized)	1.29857	2.78	4.74	13.64

Table 2. Optimized values of K_p and K_i, and the resulting performance parameters obtained by Mansor et al. [42] and Samat et al. [43].

Optimization Method	Kp	Ki	Rise Time (sec)	Settling Time (sec)	Overshoot (%)
PSO (Unloaded) (Samat et al. [43])	8.72	0.92	1.55	1.62	0.4
PSO (Loaded) (Samat et al. [43])	7.92	0.57	1.55	1.631	0.6
FLC (Unloaded) (Mansor et al. [42])	0-1	0-1	51.498×10^{-3}	1.164	0.501

can be justified by noting that the controller values in the present work were obtained at a motor dynamic speed range of 800-1200 rpm, which vary from that used by the above references.

4. Conclusion

The current investigation focuses on looking into the effect of the PI controller on the speed regulation of a DC servo motor. The study is done both experimentally and theoretically. The experimental set-up involves a servo trainer TQ CE110, an analog PID controller TQ CE120, and an analysis software CE 2000 installed in a computer. For theoretical analysis, a second-order transfer function with the Proportional (P) and Integral (I) gains terms is used. DC servo motor steady-state and transient responses in response to varying proportional and integral gains are recorded experimentally and calculated theoretically in volts by solving the transfer function in a MATLAB Simulink environment. The output in volts can easily be converted to angular velocity in rad/sec using the calibration curve obtained by Bahakeem and Jamal [68]. In addition, the effects of the damping ratio and undamped natural frequency (speed of response) controlled by the P and I controllers on motor response are also analysed. Finally, optimized values of P and I gains are found theoretically, providing the best compromise between the overshoot, peak time, rise time, and settling time of the system response.

It is found before the actual experiment and theoretical work that using a Derivative (D) controller with PI controllers to control the DC motor speed is not useful, since it is found theoretically that an increase in the derivative controller gain K_d does not eliminate the steady-state error. In addition, smaller values of it do not improve the response considerably, and larger values cause the system to respond abruptly, which is not physically viable as it can damage the motor. Therefore, D controller is not used in the analysis. Experimental and theoretical results for the steady-state input signal show that at a given K_p, an increase in the integral controller gain K_i yields a slower system response to achieve the steady-state set value of the process variable, and the number and frequency of oscillations increase. Moreover, peak time and rise time decrease. The transient system responses obtained experimentally and theoretically show that at a given K_i, a decrease in K_p reduces the system damping, which in turn increases the response overshoot. However, the natural frequency (speed of response) does not change. An increase in K_i, on the other hand, decreases the damping, peak time, and rise time, and increases the speed of response. The damping ratio is reduced by decreasing K_p. By doing so, the system response shows magnified overshoot and a somewhat increase in peak time. Also, the natural frequency is reduced by decreasing both K_p and K_i since both gains are functions of the natural frequency. The results show a delay in system response, an increase in rise time and peak time, and a decrease in overshoot. Finally, the optimized values of K_p and K_i obtained from the optimization feature of Simulink are run theoretically to compare the resulting system response with those of the experiment and theory without optimization. The ranges of K_p and K_i in CE120 analog controller imposes a limit to the theoretical analysis, which corresponds to experimental analysis for its validation. Hence, novelty of this work is providing a theoretical model of speed control of a DC servo motor with optimum values of controller gains as an alternative to the experimental procedure to obtain the desired performance of the system response. However, some unexplored avenues such as trajectory tracking and broader operating conditions to further expand the current work are the scopes for future investigation. The implications of the developed model can be marked by its ability to be extended to other electro-mechanical systems such as gas-fired water heaters, electric propulsion systems,

strip plastic production, and air-conditioning temperature control after some minor modifications.

Acknowledgement

Acknowledgments are due to Jubail Industrial College, Royal Commission for Jubail.

Statements and declarations

Competing interests

The authors have no competing interests to declare that are relevant to the content of this article.

Author contributions

The lead author, Adel S. Bahakeem conducted the experiments and MATLAB Simulink Simulations. The corresponding author Ahmad Jamal assisted the lead author in MATLAB Simulink simulations and wrote the results and discussion. Third author Mir M. M. Morshed wrote the introduction and literature review. The fourth author Elwaleed A. Khidir wrote the theoretical background.

Data availability

The datasets generated and analyzed during the current study are available in the Figshare repository, https://figshare.com/articles/dataset/PI_Controller_Characterization/24994026.

Funding

The authors did not receive financial support from any organization for the submitted work.

References

1. Zhang J, Wang N, Wang SA. Developed method of tuning PID controllers with fuzzy rules for integrating processes. In Proceedings of the American Control Conference (ACC). June 30-July 2, 2004; Boston, USA. https://doi.org/10.23919/ACC.2004.1386720.
2. Jimenez RL, Yam VMM, Cosgaya HQ, Ortiz B. Tuning of a PI controller using a multi-objective genetic algorithm applied to an experimental oven. Dyna New Technologies. 2017;4(1). https://doi.org/10.6036/NT8518.
3. Monje CA, Chen Y, Vinagre BM, Xue D, Feliu V. Fractional-order systems and controls: Fundamentals and applications. London: Springer Verlag; 2010. https://doi.org/10.1007/978-1-84996-335-0.
4. Hassan MA, Abd-El-Tawwab AM, Abd-El-Gwwad KA, Salem MMM. PI controller for active twin-accumulator suspension with optimized parameters based on a quarter model. Int J Sci Eng Res (IJSER). 2015;6(12):862–871. https://doi.org/10.48550/arXiv.1706.02147.
5. Sinthipsomboon K, Hunsacharoonroj I, Khedari J, Po-Ngaen W, Pratumsuwan P. Fuzzy controllers- recent advances in theory and applications. In A Hybrid of Fuzzy and Fuzzy Self-Tuning PID Controller for Servo Electro-Hydraulic System. London: INTECH;2012. http://dx.doi.org/10.5772/48614.
6. Lan S. The application of fuzzy self-tuning PID controller in SEHS. In Proceedings of the International Conference on Information Engineering and Applications (IEA). October 26–28, 2012; Chongqing, China. https://doi.org/10.1007/978-1-4471-4853-1_68.
7. Korayem MH, Imanian A, Tourajizadeh H, Khayatzadeh S, Maddah SME, Tajik A, Manteghi S. A method for simultaneous control of speed and torque of the motors of a cable suspended robot for racking procedure. Sci Iran, Trans. B: Mech Eng. 2013;20(5):1550–1565. http://scientiairanica.sharif.edu/article_3412.html.
8. Zheng W, Luo Y, Chen Y, Wang X. A simplified fractional order PID controller's optimal tuning: A case study on a PMSM speed servo. Entropy. 2021;23(2):130. https://doi.org/10.3390/e23020130.
9. Zheng W, Luo Y, Pi Y, Chen Y. Improved frequency-domain design method for the fractional order proportional-integral-derivative controller optimal design: A case study of permanent magnet synchronous motor speed control. IET Control Theory Appl. 2018;12(18):2478–2487. http://ieeexplore.ieee.org/document/8556561.
10. Ekinci S, Izci D, Hekimoglu B. Optimal FOPID speed control of DC motor via opposition-based hybrid manta ray foraging optimization and simulated annealing algorithm. Arab J Sci Eng. 2021;46:1395–1409. https://doi.org/10.1007/s13369-020-05050-z.
11. Ali FH, Hussein MM, Ismael SMB. Labview FPGA implementation of a PID controller for D.C. motor speed control. Iraqi J Electr Electron Eng. 2010;6(2):139–144. https://doi.org/10.37917/ijeee.6.2.9.
12. Rajasekhar A, Jatoth RK, Abraham A. Design of intelligent PID/PI$^{\lambda}$D$^{\mu}$ speed controller for chopper fed DC motor drive using opposition based artificial bee colony algorithm. Eng Appl Artif Intell. 2014;29:13–32. http://dx.doi.org/10.1016/j.engappai.2013.12.009.
13. Dawood SM, Majeed SH, Nekad HJ. PID Controller based multiple (master/slaves) permanent magnet synchronous motors speed control. Iraqi J Electr Electron Eng. 2015;11(2):183–192. https://doi.org/10.37917/ijeee.11.2.5.
14. Jarjees AM. Utilizing adaptive Tabu search technique based tuning PID controller for optimal speed control single phase induction motor. Al-Rafidain Eng. 2015;23(5):69–80. https://doi.org/10.33899/rengj.2015.108998.
15. Yazgan HR, Yener F, Soysal S, Gür AE. Comparison performances of PSO and GA to tuning PID controller for the DC motor. Sakarya Univ J Sci. 2019;192710565. https://doi.org/10.16984/saufenbilder.376464.
16. Wang S, Liang H, Wang J. GA PID control research in inverter motor speed governing system. J Comput Methods Sci Eng. 2019;19(2):299–306. https://doi.org/10.3233/JCM-180869.
17. Somwanshi D, Bundele M, Kumar G, Parashar G. Comparison of fuzzy-PID and PID controller for speed control of DC motor using LabView. Procedia Comput Sci. 2019;152:252–260. https://doi.org/10.1016/j.procs.2019.05.019.

18. Ekinci S, Izci D, Hekimoglu B. PID speed control of DC motor using Harris Hawks optimization algorithm. In Proceedings of the 2nd International Conference on Electrical, Communication, and Computer Engineering (*ICECCE*). June 12–13, 2020; Istanbul, Turkey. https://doi.org/10.1109/ICECCE49384.2020.9179308.
19. George MA, Kamat DV. Design of a Taguchi-GRA optimized PID and adaptive PID controllers for speed control of DC motor. Arch Electr Eng. 2021;70(4):759–775. https://doi.org/10.24425/aee.2021.138259.
20. Munagala VK, Jatoth RK. A novel approach for controlling DC motor speed using NARXnet based FOPID controller. Springer Nature. 2022;16:10–16. https://doi.org/10.1007/s12530-022-09437-1.
21. Liu X, Bai G. Research on intelligent algorithm of the AC motor speed regulation system based on the neural network. Mob Inf Syst. 2022;1590779. https://doi.org/10.1155/2022/1590779.
22. Babes B, Hamouda N, Albalawi F, Aissa O, Ghoneim SSM, Abdelwahab SAM. Experimental investigation of an adaptive fuzzy-neural fast terminal synergetic controller for buck DC/DC converters. Sustainability. 2022;14:7976. https://doi.org/10.3390/su14137967.
23. Swami A, Gaur P. ISTF-PID based DC servo motor control. In Proceedings of the IEEE 7th Power India International Conference (PIICON). November 25–27, 2016; Bikaner, India. https://doi.org/10.1109/POWERI.2016.8077237.
24. Meena DK, Chahar S. Speed control of DC servo motor using genetic algorithm. In Proceedings of the International Conference on Information, Communication, Instrumentation, and Control (ICICIC). August 17–19, 2017; Indore, India. https://doi.org/10.1109/ICOMICON.2017.8279122.
25. Sun H, Wang X, Lin Q, Wang X, Su S. The design of the DC servo motor controller based on fuzzy immune PID algorithm. In Proceedings of the 36th Chinese Control Conference (CCC). July 26–28, 2017; Dalian, China. https://doi.org/10.23919/CHICC.2017.8028098.
26. He S, Chen Z, Gao X. Parameter solving of DC servo motor PID controller based on improved firefly algorithm. In Proceedings of the 3rd International Conference on Robotics and Automation Engineering (ICRAE). November 17–19, 2018; Guangzhou, China. https://doi.org/10.1109/ICRAE.2018.8586756.
27. Kumar V, Mittal M. Optimal speed control of DC servomotor in the presence of disturbance and noise using stochastic algorithm. In Proceedings of the 3rd International Conference on Trends in Electronics and Informatics (ICOEI). April 23–25, 2019; Tirunelveli, India. https://doi.org/10.1109/ICOEI.2019.8862605.
28. Polsena A, KongJeen Y, Watcharakhup S. Identifying parameter and PI tuning of DC motor for predict behavior based on PSO. In Proceedings of the 9th International Electrical Engineering Congress (IEECON). March 10–12, 2021; Pattaya, Thailand. https://doi.org/10.1109/iEECON51072.2021.9440341.
29. Kociszewski R. Implementation of PI controller in reconfigurable PSoC microcontroller to control the speed of mobile robot drives. In Proceedings of the 2020 International Conference on Mechatronic Systems and Materials (MSM). July 1–3, 2020; Bialystok, Poland. https://doi.org/10.1109/MSM49833.2020.9202384.
30. Yustin AS, Nugroho H, Wibowo WK. Precise speed control of DC motor by implementing cascade PI controller. In Proceedings of the IEEE International Conference on Automatic Control & Intelligent Systems (I2CACIS). June 26, 2021; Online. https://doi.org/10.1109/I2CACIS52118.2021.9495889.
31. Sundareswaren K, Vasu M. Genetic tuning of PI controller for speed control of DC motor drive. In Proceedings of the IEEE International Conference on Industrial Technology (ICIT). January 19–22, 2000; Goa, India. https://doi.org/10.1109/ICIT.2000.854212.
32. Kumar CA, Nair NK. Multi-objective PI controller design with an application to speed control of permanent magnet DC motor drives. In Proceedings of the International Conference on Signal Processing, Communication, Computing, and Networking Technologies (ICSCCN). July 21-22, 2011; Thuckalay, India. https://doi.org/10.1109/ICSCCN.2011.6024588.
33. Kanojiya RG, Meshram PM. Optimal tuning of PI controller for speed control of DC motor drive using particle swarm optimization. In Proceedings of the International Conference on Advances in power Conversion and Energy Technologies (APCET). August 2–4, 2012; Mylavaram, India. https://doi.org/10.1109/APCET.2012.6302000.
34. Ozturk N. Speed control for DC motor drive based on fuzzy and genetic PI controller – A comparative study. Electron Elect Eng. 2012;7(123):43–48. http://dx.doi.org/10.5755/j01.eee.123.7.783.
35. Ahmed A, Mohan Y, Chauhan A, Sharma P. Comparative study of speed control of DC motor using PI, IP, and fuzzy controller. Int J Adv Res Comp Comm Eng. 2013;2(7):2693–2697. https://doi.org/10.17148/IJARCCE.2019.81216.
36. Khan HS, Kadri MB. DC motor speed control by embedded PI controller with hardware-in-loop simulation. In Proceedings of the 3rd IEEE International Conference on Computer, Control, & Communication (IC4). September 25–26, 2013; Karachi, Pakistan. https://doi.org/10.1109/IC4.2013.6653742.
37. Daksha N, Rudraksha K. Design and testing of self-tuned fuzzy PI controller for improved speed control and accelerating torque characteristics of a DC motor. In Proceedings of the 4th International Conference on Power, Control, & Embedded Systems (ICPCES). March 9–11, 2017; Allahabad, India. https://doi.org/10.1109/ICPCES.2017.8117651.
38. Bosco MC, Guedes JJ, Castoldi MF, Goedtel A, Pires da Silva ER, Buzachero LFS. Estimation of parameters and tuning of a speed PI of permanent magnet DC motor using differential evolution. In Proceedings of the 2017 IEEE International Electric Machines and Drives Conference (IEMDC). May 21–24, 2017; Miami, USA. https://doi.org/10.1109/IEMDC.2017.8002318.
39. Naung Y, Anatolii S, Lin YH. Speed control of DC motor by using neural network parameter tuner for PI-controller. In Proceedings of the 2019 IEEE Conference of Russian Young Researchers in Electrical and Electronic Engineering (EIConRus). January 28–31, 2019; Moscow, Russia. https://doi.org/10.1109/EIConRus.2019.8656911.
40. Firmansyah R, Irmawanto R. Comparison study of PI controller tuning method to regulate the DC motor speed. In Proceedings of the 3rd International Conference on Research and Academic Community Services (ICRACOS). October 9–10, 2021; Surabaya, Indonesia. https://doi.org/10.1109/ICRACOS53680.2021.9702007.
41. Semenov AS, Semenova MN, Bebikhov YV. Mathematical simulation of a PI speed controller for a separately excited DC motor. In Proceedings of the International Ural Conference on Electrical Power Engineering (UralCon). September 24-26, 2021; Magnitogorsk, Russian Federation. https://doi.org/10.1109/UralCon52005.2021.9559518.

42. Mansor MN, Samat AAA, Tajudin AI, Salim NA, Daud K, Shukor FA. Self tuning of PI controller for speed control of DC motor by using fuzzy logic controller. In Proceedings of the 6th IEEE International Conference on Recent Advances and Innovations in Engineering (ICRAIE). December 1-3, 2021; Kedah, Malaysia. https://doi.org/10.1109/ICRAIE52900.2021.9703980.
43. Samat AAA, Subani MA, Aziz NFA, Salim NA, Daud K, Tajudin AI. PSO-based PI controller for speed control of DC motor. In Proceedings of the 2022 IEEE International Conference on Power and Energy (PECon). December 5–6, 2022; Kedah, Malaysia. https://doi.org/10.1109/PECon54459.2022.9988840.
44. Tufenkci S, Alagoz BB, Kavuran G, Yeroglu C, Herencsar N, Mahata S. Theoretical demonstration for reinforcement learning of PI control dynamics for optimal speed control of DC motors by using twin delay deep deterministic policy gradient algorithm. Expert Syst Appl. 2023;213:119192. https://doi.org/10.101/j.eswa.2022.119192.
45. Alejandro-Sanjines U, Maisincho-Jivaja A, Asanza V, Lorente-Leyva LL, Peluffo-Ordonez DH. Adaptive PI controller based on a reinforcement learning algorithm for speed control of a DC motor. Biomimetics. 2023;8:434. https://doi.org/10.3390/biomimetics8050434.
46. Çelik E, Öztürk N. First application of symbiotic organisms search algorithm to off-line optimization of PI parameters for DSP-based DC motor drives. Neural Comput. & Appl. 2018;30(9). https://doi.org/10.1007/s00521-017-3256-5.
47. Celik E, Gör H. Enhanced speed control of a DC servo system using PI + DF controller tuned by stochastic fractal search technique. J. Franklin Inst. 2019;356(3):1333–1359. https://doi.org/10.1016/j.jfranklin.2018.11.020.
48. Celik, E., Bal G, Ozturk N, Bekiroglu E, Houssein EH, Ocak C, Sharma G. Improving speed control characteristics of PMDC motor drives using nonlinear PI control. Neural Comput. & Appl. 2024;36:9113–9124. https://doi.org/10.1007/s00521-024-09568-3.
49. Çelik E, Öztürk, N. Optimal setting of PI parameters for direct current motor drives by symbiotic organisms search algorithm. Bilisim Teknolojileri Dergisi. 2017;10(3):311–318. https://doi.org/10.17671/gazibtd.331044.
50. Tariq M, Bhattacharya TK, Varshney N, Rajapan D. Fast response antiwindup PI speed controller of brushless DC motor drive: Modeling, simulation, and implementation on DSP. J Electr Syst Inf Technol. 2016;3:1–13. https://doi.org/10.1016/j.jesit.2015.11.008.
51. Verma V, Harish V, Bhardwaj R. Hybrid PI speed controllers for permanent magnet brushless DC motor. In Proceedings of the 5th IEEE India International Conference on Power Electronics (IICPE). December 6–8, 2012; Delhi, India. https://doi.org/10.1109/IICPE.2012.6450500.
52. Shyam A, Daya JLF. A comprehensive study on the speed response of BLDC motor using conventional PI controller, antiwindup PI controller and fuzzy controller. In Proceedings of the International Conference on Control Communication and Computing (ICCC). December 13–15, 2013; Thiruvananthapuram, India. https://doi.org/10.1109/ICCC.2013.6731626.
53. Soorya K, Steffy SA. Analysis and simulation of speed control of PMBLDC motor by PI controller. In Proceedings of the International Conference on Green Computing Communication and Electrical Engineering (ICGCCEE). March 6–8, 2014; Coimbatore, India. https://doi.org/10.1109/ICGCCEE.2014.6922431.
54. Khanke PK, Jain SD. Comparative analysis of speed control of BLDC motor using PI, simple FLC, and fuzzy-PI controller. In Proceedings of the International Conference on Energy Systems and Applications (ICESA). October 30-November 1, 2015; Pune, India. https://doi.org/10.1109/ICESA.2015.7503359.
55. John GS, Vijayan AT. Anti-windup PI controller for speed control of brushless DC motor. In Proceedings of the IEEE International Conference on Power, Control, Signals, and Instrumentation Engineering (ICPCSI). September 21–22, 2017; Chennai, India. https://doi.org/10.1109/ICPCSI.2017.8391874.
56. Baharudin NN, Ayob SM. Brushless DC motor speed control using single input fuzzy PI controller. Int J Power Electron Drive Syst (IJPEDS). 2018;9(4):1952–1966. https://doi.org/10.11591/ijpeds.v9.i4.pp1952-1966.
57. Wongkhead S, Tunyasrirut S, Permpoonsinsup W, Puangdownreong D. State space model for BLDC motor based on digital signal processors TMS320F28335 for speed control by using proportional Integral controller. In Proceedings of the 7th International Electrical Engineering Congress (IEECON). March 6–8, 2019; Hua Hin, Thailand. https://doi.org/10.1109/iEECON45304.2019.8938880.
58. Khaniki MAL, Esfandiari S, Manthouri M. Speed control of brushless DC motor using fractional order fuzzy PI controller optimized via WOA. In Proceedings of the 10th International Conference on Computer and knowledge Engineering (ICCKE). October 29–30, 2020; Mashhad, Iran. https://doi.org/10.1109/ICCKE50421.2020.9303634.
59. Wang T, Wang H, Hu H, Wang C. LQR optimized BP neural network PI controller for speed control of brushless DC motor. Adv Mech Eng. 2020;12(10):1–13. https://doi.org/10.1177/1687814020968980.
60. Beladjine DE, Boudana D, Moualdia A, Hallouz M, Wira P. A comparative study of BLDC motor speed control using PI and ANN regulator. In Proceedings of the 18th International Multi-Conference on Systems, Signals, & Devices (SSD). March 22–25, 2021; Monastir, Tunisia. https://doi.org/10.1109/SSD52085.2021.9429474.
61. Sandip R, Karthik N, Getzial Anbu Mani T. PSO based PI controller for BLDC motor. In Proceedings of the 8th International Conference on Smart Structures and Systems (ICSSS). April 21–22, 2022; Chennai, India. https://doi.org/10.1109/ICSSS54381.2022.9782223.
62. Sarkar P, Pal S, Das SS. Parameter estimation and speed control of PMDC servo motor using method of time moments. Sens transducers. 2010;119(8):162–173. http://www.sensorportal.com.
63. Hote YV, Saxena S, Jha AN. Controller design via reduced model for DC servo system: An experimental study. In Proceedings of the IEEE 10th International Conference on Industrial and Information Systems (ICIIS 2015). December 18–20, 2015; Peradeniya, Sri Lanka. https://doi.org/10.1109/iciinfs.2015.7399045.
64. Rai A, Das DK, Lotha MM. LabView platform based real-time speed control of a DC servo motor with fuzzy-PI controller. In Proceedings of the International Conference on Electrical, Electronics, and Computer Engineering (UPCON). November 8–10, 2019; Aligarh, India. https://doi.org/10.1109/UPCON47278.2019.8980036.
65. Fayad SA, Shaban M, Attia M, Abdelwahab SAM. Performance enhancement of speed and position control for DC servo motor using artificial intelligence technique. Int J Electr Eng Inform (IJEEI). 2022;14(3):552–566. https://doi.org/10.15676/ijeei.2022.14.3.4.
66. Mohamed M, Alaas ZM, Faiya B A, Hegazy H Y, Mohamed W I, Abdelwahab S A M. Performance improvement of grid-connected PV-wind hybrid systems using adaptive

neuro-fuzzy inference system and fuzzy FOPID advanced control with OPAL-RT. IEEE Access. 2025;13:55996–56020. https://doi.org/10.1109/ACCESS.2025.3548926.
67. TecQuipment. User manual for TQ CE110 servo trainer. 2010; TecQuipment Ltd.
68. Bahakeem AS, Jamal, A. Experimental investigation of the proportional controller-based model of DC servo motor. Int J Sci Res (IJSR). 2021;10(8):1171–1177. https://doi.org/10.21275/SR21825170847.
69. Abdelwahab SAM, El-Rifaie AM, Hegazy HY, Tolba MA, Mohamed WI, Mohamed M. Optimal control and optimization of grid-connected PV and wind turbine hybrid systems using electric eel foraging optimization algorithms. Sensors. 2024;24:2354. https://doi.org/10.3390/s24072354.

Appendix 1

Dynamic response

The closed-loop transfer function to represent the speed control of servo motor is given as [67],

$$y_\omega(s) = \frac{K(s)\,G_1(s)\,y_r(s)}{1 + K(s)\,G_1(s)} \tag{16}$$

where $K(s)$ represents a general notation for controller transfer function and y_r represents the potentiometer reference speed signal. If both the proportional and integral controllers are considered, the expression of $K(s)$ becomes [67],

$$K(s) = K_p + \frac{K_i}{s} \tag{17}$$

The standard linear transfer function is given by [67],

$$y_\omega(s) = \frac{G_1}{Ts+1} v(s) \tag{18}$$

The derivation of this transfer function can be seen in detail in [67]. The block diagram of velocity control servo system (Fig. 1) shows the linear transfer function as,

$$y_\omega(s) = G_1(s)\,v(s) \tag{19}$$

Comparing the standard eq. (A.3) with eq. (A.4) yields the expression of speed transfer function $G_1(s)$ as,

$$G_1(s) = \frac{G_1}{Ts+1} \tag{20}$$

Substituting the expressions of $K(s)$ from eq. (A.2) and $G_1(s)$ from eq. (A.5) in eq. (A.1) yields,

$$y_\omega(s) = \left[\frac{\left(K_p + \frac{K_i}{s}\right)\left(\frac{G_1}{Ts+1}\right)}{1 + \left(K_p + \frac{K_i}{s}\right)\left(\frac{G_1}{Ts+1}\right)}\right] y_r(s)$$

$$y_\omega(s) = \left[\frac{\left(\frac{K_p.s+K_i}{s}\right)\left(\frac{G_1}{Ts+1}\right)}{1 + \left(\frac{K_p.s+K_i}{s}\right)\left(\frac{G_1}{Ts+1}\right)}\right] y_r(s)$$

$$y_\omega(s) = \left[\frac{\frac{(K_p.s+K_i)G_1}{s(Ts+1)}}{\frac{s(Ts+1)+K_p.sG_1+K_iG_1}{s(Ts+1)}}\right] y_r(s)$$

$$y_\omega(s) = \left[\frac{\left(K_i + K_p.s\right)G_1}{Ts^2 + s + K_p.sG_1 + K_iG_1}\right] y_r(s)$$

$$y_\omega(s) = \left[\frac{\left(K_i + K_p.s\right)G_1}{Ts^2 + \left(1 + K_p.G_1\right)s + K_iG_1}\right] y_r(s) \tag{21}$$

The values of motor gain, $G_1 = 1.0059$ and time constant, $T = 1.60$ are obtained, experimentally, using TecQuipment servo trainer apparatus, TQ CE110 and analog controller, TQ CE120 with largest inertial load

and clutch disengaged. The value of G_1 is obtained by determining the slope of the curve of motor sensor output vs the motor drive voltage. In addition, T is obtained by noting the time corresponding to 63.2% of the steady-state response of servo motor plotted against time subjected to step input signal [68]. Finally, substituting the obtained values of $G_1 = 1.0059$ and $T = 1.60$ in eq. (A.6) yields,

$$y_\omega(s) = \left[\frac{\left(K_i + K_p.s\right)1.0059}{1.60s^2 + \left(1 + 1.0059K_p\right)s + 1.0059K_i}\right] y_r(s)$$